

---

# GRU: MITIGATING THE TRADE-OFF BETWEEN UNLEARNING AND RETENTION FOR LARGE LANGUAGE MODELS

---

Yue Wang<sup>1</sup> Qizhou Wang<sup>1</sup> Feng Liu<sup>2</sup> Wei Huang<sup>3</sup> Yali Du<sup>4</sup> Xiaojiang Du<sup>5</sup> Bo Han<sup>1</sup>

<sup>1</sup>TMLR Group, Department of Computer Science, Hong Kong Baptist University

<sup>2</sup>The University of Melbourne

<sup>3</sup>RIKEN Center for Advanced Intelligence Project

<sup>4</sup>King's College London

<sup>5</sup>Department of Electrical and Computer Engineering, Stevens Institute of Technology

## ABSTRACT

Large language model (LLM) unlearning has demonstrated its essential role in removing privacy and copyright-related responses, crucial for their legal and safe applications. However, the pursuit of complete unlearning often comes with substantial costs due to its compromises in their general functionality, leading to a notorious trade-off between unlearning and retention. In examining the update process for unlearning dynamically, we find gradients hold essential information for revealing this trade-off. In particular, we look at the varying relationship between retention performance and directional disparities between gradients during unlearning. It motivates the sculpting of an update mechanism derived from gradients from two sources, i.e., harmful for retention and useful for unlearning. Accordingly, we propose Gradient Rectified Unlearning (GRU), an enhanced unlearning framework controlling the updating gradients in a geometry-focused and optimization-driven manner such that their side impacts on other, unrelated responses can be minimized. Specifically, GRU derives a closed-form solution to project the unlearning gradient onto the orthogonal space of that gradient harmful for retention, ensuring minimal deviation from its original direction under the condition that overall performance is retained. Comprehensive experiments are conducted to demonstrate that GRU, as a general framework, is straightforward to implement and efficiently enhances a range of baseline methods through its adaptable and compatible characteristics. Additionally, experimental results show its broad effectiveness across a diverse set of benchmarks for LLM unlearning.

## 1 Introduction

Large language models (LLMs)[1, 2] have revolutionized the learning paradigms towards general-purpose language generation and understanding, enabling new frontiers in linguistic adaptability, knowledge representation, and advanced reasoning. These models typically employ architectures based on multi-head attention decoders with billions of learnable parameters and are trained autoregressively on web-derived datasets containing trillions of tokens [3]. Such substantial scaling equips LLMs to tackle a wide array of complex linguistic tasks, thereby demonstrating remarkable capabilities that span diverse domains such as programming, creative writing, and scientific research [4, 5, 6, 7].

While scaling offers remarkable benefits, it also introduces substantial drawbacks. A primary concern is the propensity of LLMs to memorize data [8, 9], potentially reproducing sensitive messages encountered during its pre-training. It encompasses copyright and privacy-related issues [10, 11], highlighting concerns about the potential misuse of LLMs for illicit activities as well as challenges in safeguarding individual rights [12]. Therefore, LLMs should be used in accordance with ethical and legal principles. To remove these undesirable behaviors, it is essential to conduct regular audits to identify sensitive content and subsequently adjust the embedded knowledge within LLMs by removing them.

As the key technique to achieve this goal, LLM unlearning [11, 13] explores strategies to remove parameterized knowledge targeted to be unlearned directly. One of the foundational methods is gradient ascent (GA) [13], which

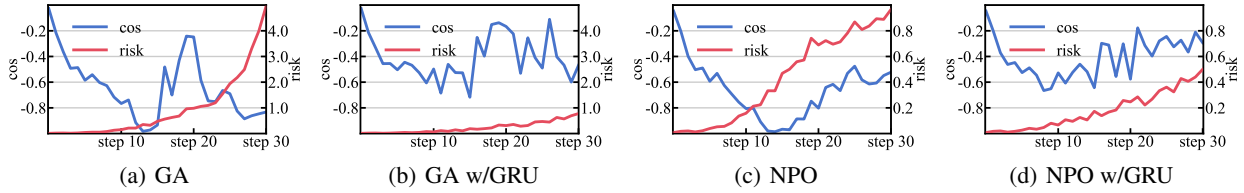


Figure 1: **Illustration of gradient dynamics during the unlearning process.** We visualize the cosine similarity (denoted as “cos”) between gradients computed on retain and unlearning data, alongside the corresponding retention performance (measured by the cross-entropy loss on retain data, referred to as “risk”) under the TOFU 5% dataset. In the experiment, we followed the configuration described in Section 5. Panels (a) and (c) illustrate the relationship between gradient direction alignment and retention performance during unlearning with GA and NPO. The cosine similarity declines drastically as unlearning starts, reflecting an increasing directional discrepancy between gradients computed from retain and unlearning data. Retention performance deteriorates correspondingly, with the two curves crossing each other. Panels (b) and (d) illustrate the gradient dynamics for both methods with GRU gradient rectification. The deviation in both the cosine similarity and retention performance is clearly lowered. Specifically, we observe that the cosine similarity and risk curves remain stable and do not intersect.

directly minimizes the log-likelihood for targeted data, thereby reducing their probabilities of being generated to nearly zero. However, GA has notably negative impacts on model responses for other, non-targeted data, spurring subsequent work that regularizes unlearning procedures to retain overall model behaviors [14, 15, 16]. However, there remains an inherent trade-off between unlearning and retention, in which preserving common performance comes at the cost of reducing the effectiveness of unlearning [11, 15]. Consequently, we are motivated to raise a pivotal research question:

*How can we mitigate the trade-off between the process of unlearning and the goal of retaining overall performance?*

We first conduct observational experiments to better understand the model update dynamics during the unlearning process. Specifically, we delve into the fundamental component—model gradients. To do so, we separately compute the gradients of the current model on retain (non-targeted) and unlearning (targeted) data<sup>1</sup>, and measure their directional alignment using cosine similarity. Additionally, we track the corresponding retention performance to clearly illustrate how gradient alignment affects the model’s behavior throughout unlearning. In Figure 1, we present two representative pairs of visualizations, illustrating these gradient dynamics and retention performance for the representative unlearning methods GA and Negative Preference Optimization (NPO) [15]. This empirical observation motivated the design of our framework. In the following sections, we further substantiate this motivation through a formal and theoretical analysis.

To this end, we introduce the Gradient Rectified Unlearning (GRU), a general framework to mitigate the trade-off between unlearning and retention with both optimisation and geometry implications. The key insight of GRU lies in the gradient rectification during model updates: The gradients for unlearning are re-projected onto the orthogonal directions with respect to those that are detrimental to retention, thereby ensuring the overall intact performance under a first-order assumption (cf., Section 3.1). Accordingly, examples illustrating the altered behavior of gradient dynamics are shown in Figure 1(b) and (d). The directions that potentially harm retention can be estimated by the gradients from a set of data non-targeted for unlearning, which are readily accessible for many well-established benchmarks [14] or can be directly extracted from pre-trained models [17]. Please refer to Figure 2 for a conceptual illustration of our framework.

We further provide a detailed analysis to comprehend the mechanisms behind GRU. For the goal of retention, we

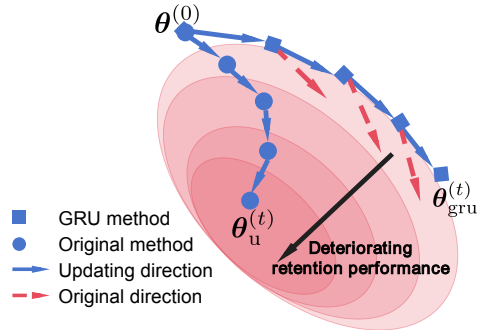


Figure 2: **Conceptual illustration of our unlearning framework.** Conventional unlearning methods, such as GA, often suffer from declining retention performance, leading to diminished model utility. GRU mitigates this issue by rectifying the original gradients at each step, ensuring reliable unlearning without compromising retention performance.

<sup>1</sup>We adopt the term “retain data” to align with existing literature (e.g., the TOFU benchmark [14]), and also because pairing “retain data” with “unlearning data” improves readability and closely reflects the core theme of our work. In particular, we refer to data not targeted to be unlearned as “retain data,” and data targeted to be unlearned as “unlearning data,” throughout this paper.

demonstrate that GRU offers enhanced reliability over previous unlearning methods. Therein, accurately estimating the retention direction is key to a successful outcome. For the goal of unlearning, those original methods that possess closer gradient directions (i.e., smaller cosine similarity) to that for retention lead to better effectiveness, thereby allowing the rectified unlearning gradients to maintain a substantial magnitude after adjustment. Hence, a proper choice of fundamental unlearning methods remains equally essential. Additionally, a further consideration is that retain data can often be biased in real scenarios. Developing methods independent of retain data is appealing while maintaining retention performance. With the theoretical insight, we can easily arrive at a variant of GRU, task vector rectified unlearning (TRU), with the same optimization mechanism that can easily adapt to challenging retain-data-free setting.

We conduct comprehensive experiments in a variety of well-established unlearning benchmarks, including TOFU [14], WMDP [18], and MUSE [19]. The integration of our GRU with established baselines demonstrates its effectiveness, achieving powerful unlearning capabilities alongside enhanced retention reliability. We also compare TRU with different competitive methods, and its superiority reveals a promising direction of efforts. These results highlight the generality and substantial potential of our approach in effectively mitigating the trade-off between unlearning and retention.

## 2 Preliminaries

We consider a pre-trained LLM that models an autoregressive distribution over sequences of tokens. Specifically, for an input sequence  $\mathbf{s} = [s_1, s_2, \dots, s_{|\mathbf{s}|}]$ , the probability of the sequence is modeled as the product of conditional probabilities of each token given all preceding tokens:

$$p(\mathbf{s}; \boldsymbol{\theta}) = \prod_{i=1}^{|\mathbf{s}|} p(s_i | \mathbf{s}_{1:i-1}; \boldsymbol{\theta}),$$

where  $\boldsymbol{\theta}$  denotes model parameters, and  $\mathbf{s}_{1:i-1}$  represents the subsequence consisting of tokens  $s_1$  through  $s_{i-1}$ .  $\boldsymbol{\theta}$  is typically learned by minimizing the negative log-likelihood (NLL) loss over a large corpus of web-sourced data  $\mathcal{D}_t = \{\mathbf{s}^1, \mathbf{s}^2, \dots, \mathbf{s}^m\}$  of size  $m$ , which is given by  $-1/m \sum_{\mathbf{s} \in \mathcal{D}_t} \log p(\mathbf{s}; \boldsymbol{\theta})$ . Pre-trained LLMs have shown their remarkable capabilities [20]. However, these models also face safety concerns due to their reliance on web-sourced data, potentially leading to privacy breaches [21], copyright infringement [22], and potential misuse [23].

### 2.1 LLM Unlearning

These concerns motivate emerging studies of LLM unlearning recently, which aims to effectively remove undesirable data points or entire hazardous domains from original models. Formally, let  $\mathcal{D}_u = \{\mathbf{s}_u^1, \mathbf{s}_u^2, \dots, \mathbf{s}_u^n\}$  represents the unlearning dataset, typically a subset of the training data  $\mathcal{D}_t$  where  $n \ll m$ . The primary objectives of LLM unlearning are twofold [11]: **a) Removal:** The unlearned model, characterized by parameters  $\boldsymbol{\theta}_u$ , should eliminate the knowledge associated with  $\mathcal{D}_u$ , thereby reducing its capacity to recall or reproduce any information targeted to be forgotten. **b) Retention:** The model should retain its performance on the remaining data  $\mathcal{D}_t \setminus \mathcal{D}_u$ , ensuring that the capabilities on tasks and data unrelated to the unlearning dataset can be preserved in reliable manner. The objectives of removal and retention are both essential for LLM unlearning, which can be interpreted as a bi-objective learning problem [11, 24].

### 2.2 Unlearning Methods

In the following, we present several representative methods for unlearning, each addressing ways to remove or preserve retention performance, while striving to mitigating the trade-off between the two goals.

**Gradient ascent (GA)** is one of the most fundamental unlearning methods, which minimizes the log-likelihood for targeted data. The unlearning objective of GA is

$$\min_{\boldsymbol{\theta}} \mathcal{L}_{\text{GA}}(\mathcal{D}_u; \boldsymbol{\theta}) := \frac{1}{n} \sum_{\mathbf{s} \in \mathcal{D}_u} \log p(\mathbf{s}; \boldsymbol{\theta}), \quad (1)$$

which directly reduces the probabilities of generating contents resembling  $\mathcal{D}_u$  to approach zero, thereby leading to effective knowledge removal. However, due to its extremely large strengths of gradient updates, the resulting GA-unlearned models will suffer from excessive unlearning [11], where the model responses for non-targeted data will also be damaged, and thus it is clear that GA fails at retention performance. This motivates a series of subsequent works in order to improve the retention performance of the resulting models as a result of the study.

**Gradient Difference (GD)** regularizes GA with a retain dataset  $\mathcal{D}_r$  of size  $m'$ , typically sampled from  $\mathcal{D}_t \setminus \mathcal{D}_u$  and  $m' \ll m$ . These data represent the knowledge that should be preserved. The associated retain loss, which is given by

$$\mathcal{R}(\mathcal{D}_r; \theta) = -\frac{1}{m'} \sum_{s \in \mathcal{D}_r} \log p(s; \theta), \quad (2)$$

serves as regularization in conjunction with GA, namely,

$$\min_{\theta} \mathcal{L}_{\text{GD}}(\mathcal{D}_u, \mathcal{D}_r; \theta) := \mathcal{L}_{\text{GA}}(\mathcal{D}_u; \theta) + \lambda \mathcal{R}(\mathcal{D}_r; \theta), \quad (3)$$

where  $\lambda$  is a trade-off hyper-parameter, typically set to 1. However, many previous works [14] reveal that the unlearning term, i.e.,  $\mathcal{L}_{\text{GA}}(\mathcal{D}_u; \theta)$ , tends to dominate the dynamics of gradient updates. Therefore, GD may still strongly impact retention performance negatively.

**Negative Preference Optimization (NPO)** [15] directly refines the objective of GA to mitigate excessive unlearning, of which the formulation is motivated by direct preference optimization, a well-known preference alignment method [25]. NPO segregates the dis-preferred part from DPO, heuristically employing it as the unlearning objective, following the formulation of

$$\min_{\theta} \mathcal{L}_{\text{NPO}}(\mathcal{D}_u; \theta) := \frac{1}{n} \sum_{s \in \mathcal{D}_u} \frac{2}{\beta} \log \left[ 1 + \left( \frac{p(s; \theta)}{p(s; \theta_{\text{org}})} \right)^{\beta} \right], \quad (4)$$

where  $\beta$  is the inverse temperature and  $\theta_{\text{org}}$  denotes model parameters before unlearning. The effects of NPO in mitigating excessive unlearning can be understood through its gradients, which are equivalent to GA with extra reweighting [15]. This weighting mechanism pays more attention to data that have small impacts on retention. However, the strength of unlearning for NPO is weaker than that for GA, which could lead to inadequate unlearning.

**Unlearning with Control (UWC)** [16] suggests a post-unlearning calibration framework. UWC blends model parameters from before and after unlearning to restore retention performance. With a meticulous-searched controlling parameter  $\alpha$ , we have the calibrated model of

$$\alpha \theta_u + (1 - \alpha) \theta_{\text{org}}, \quad (5)$$

whose performance on  $\mathcal{D}_t \setminus \mathcal{D}_f$  can approach that of  $\theta_{\text{org}}$ . Despite UWC’s flexibility in accommodating a wide range of unlearning methods, its ability to deal with excessive unlearning still comes at the expense of compromises in the effects of unlearning, as it also supports various unlearning methods, alongside its abilities to handle excessive unlearning.

### 3 Gradient Rectified Unlearning

As discussed above, many methods have been developed to mitigate excessive unlearning. However, these achievements often result in an inevitable trade-off between removal and retention—improvements in maintaining the overall performance typically occur at the expense of weakened strength of unlearning. Considering that both goals of removal and reliable retention, are necessary to unlearn practical LLM, this trade-off is detrimental to practical LLM unlearning. If the model is compromised on removal, then privacy breaches and harmful behaviors may result; if the model is compromised on retention, it may adversely affect the model’s overall utility, adversely affecting its commercial value.

In this paper, rather than developing new methods that can better balance the trade-off between removal and retention, we turn our focus toward directly breaking this dichotomy. To put it another way, it is our intention to explore frameworks that are capable of delivering improved unlearning without compromising the overall utility of the model.

#### 3.1 Motivation and The Proposed Framework

In this section, we formalize our goal towards avoiding trade-offs by studying a constrained gradient updating rule.

To begin with, considering any unlearning objective  $\mathcal{R}_u$  mentioned in Section 2, we recall the conventional stochastic updating rule at the  $t$ -th step in the following:

$$\theta^{(t+1)} \leftarrow \theta^{(t)} - \text{lr} \cdot \mathbf{g}_u^{(t)}. \quad (6)$$

Therein,  $\text{lr}$  denotes the (un) learning rate and  $\mathbf{g}_u^{(t)} = \nabla_{\theta} \mathcal{L}(\tilde{\mathcal{D}}_u^{(t)}; \theta^{(t)})$  with  $\tilde{\mathcal{D}}_u^{(t)}$  the mini-batch of size  $b$  sampled from  $\mathcal{D}_u$  and  $\mathcal{L}$  being any unlearning loss mentioned in Section 2, e.g., GA, GD, or NPO. This direct updating rule has proven to be unreliable in terms of retention, leading to the undesirable trade-off between retention and removal, which is widely mentioned in many previous works [11, 14, 16].

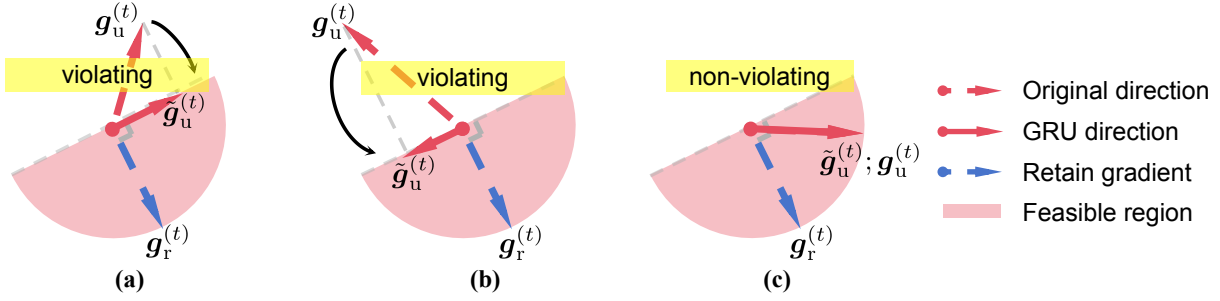


Figure 3: **Illustration of GRU Updating Rule.** Panels (a)-(b) display situations where the angles between the gradient vectors (red dashed and blue dashed arrows) are obtuse, violating the constraint in Eq. (7). In these cases, the gradients should be projected onto the orthogonal plane of the conflicting retain gradient. Panel (c) illustrates a scenario with an acute angle between the gradient vectors, adhering to the constraint in Eq. (7) and falling within the retention-safe feasible region (red half-circle), thus requiring no further adjustment.

This notable drawback motivates us to replace  $\mathbf{g}_u^{(t)}$  in Eq. (6) with its constrained version  $\tilde{\mathbf{g}}_u^{(t)}$ : We incorporate the retain loss  $\mathcal{R}$  as in Eq. (2), along with the corresponding gradients  $\mathbf{g}_r^{(t)} = \nabla_{\theta} \mathcal{R}(\mathcal{D}_r; \theta^{(t)})$ , typically estimated by random mini-batch drawn from  $\mathcal{D}_r$ . Then, we assert that the adjusted gradients  $\tilde{\mathbf{g}}_u^{(t)}$  should meet the condition as

$$\begin{aligned} \arg \min_{\tilde{\mathbf{g}}_u^{(t)}} \quad & \|\tilde{\mathbf{g}}_u^{(t)} - \mathbf{g}_u^{(t)}\|^2 \\ \text{s.t.} \quad & \langle \tilde{\mathbf{g}}_u^{(t)}, \mathbf{g}_r^{(t)} \rangle \geq 0. \end{aligned} \quad (7)$$

The objective  $\min \|\tilde{\mathbf{g}}_u^{(t)} - \mathbf{g}_u^{(t)}\|^2$  ensures that the constrained gradients remain close to their original values. Meanwhile, the constraint  $\langle \tilde{\mathbf{g}}_u^{(t)}, \mathbf{g}_r^{(t)} \rangle \geq 0$  guarantees that there will be no adverse effect on model performance in retain data after updates. Overall, Eq. (7) encapsulates our principle that the removal of targeted knowledge should occur under strict conditions that ensure the retention performance on non-targeted data, thereby mitigating the inherent trade-off associated with such an approach. It is our intention to mitigate the trade-off by adjusting the gradient direction, hence we name the proposed unlearning framework as **gradient rectified unlearning (GRU)**.

The rationale behind  $\langle \tilde{\mathbf{g}}_u^{(t)}, \mathbf{g}_r^{(t)} \rangle \geq 0$  for retention is simple: Assuming the model is locally linear [26], we can approximate the expected loss change for the retain data as  $\mathcal{R}(\theta + 1r \cdot \tilde{\mathbf{g}}_u) - \mathcal{R}(\theta) \approx 1r \langle \tilde{\mathbf{g}}_u^{(t)}, \mathbf{g}_r^{(t)} \rangle$ . As observed, a positive  $\langle \tilde{\mathbf{g}}_u^{(t)}, \mathbf{g}_r^{(t)} \rangle$  implies that the loss  $\mathcal{R}$  does not deteriorate following gradient updates, thereby ensuring the goal of retention. Later, we will show that the condition expressed in Eq. (7) remains valid under some less stringent assumptions, demonstrating its practical applicability and highlighting the validity of the method.

### 3.2 Realizations

Throughout this section we will explore details on how to implement GRU, focusing on the closed-form solution that GRU provides as well as additional strategies to enhance its reliability in the field.

**Closed-form solution.** Eq. (7) is a constrained optimization problem that is not easy to be implemented. However, it constitutes a quadratic programming problem with a linear constraint, allowing us to derive its closed-form solution. Specifically, the adjustment gradients can be written as:

$$\begin{aligned} \tilde{\mathbf{g}}_u^{(t)} &= \mathbf{g}_u^{(t)} + \frac{\max(-\langle \mathbf{g}_u^{(t)}, \mathbf{g}_r^{(t)} \rangle, 0)}{\|\mathbf{g}_r^{(t)}\|^2} \mathbf{g}_r^{(t)} \\ &= \mathbf{g}_u^{(t)} + \frac{\|\mathbf{g}_u^{(t)}\| \max(-\cos(\mathbf{g}_u^{(t)}, \mathbf{g}_r^{(t)}), 0)}{\|\mathbf{g}_r^{(t)}\|} \mathbf{g}_r^{(t)}, \end{aligned} \quad (8)$$

where  $\cos(\mathbf{g}_u^{(t)}, \mathbf{g}_r^{(t)}) = \langle \mathbf{g}_u^{(t)}, \mathbf{g}_r^{(t)} \rangle / (\|\mathbf{g}_u^{(t)}\| \cdot \|\mathbf{g}_r^{(t)}\|)$ . For more detailed derivations, please refer to Appendix A.1.

Eq. (8) conveys a clear geometric interpretation, adjusting the original gradients  $\mathbf{g}_u^{(t)}$  onto the half-space defined by the constraint  $\langle \mathbf{g}_u^{(t)}, \mathbf{g}_r^{(t)} \rangle \geq 0$ . If this constraint is already satisfied, then  $\mathbf{g}_u^{(t)}$  remains unchanged. Otherwise,  $\mathbf{g}_u^{(t)}$  will be

**Algorithm 1** GRU Framework

---

```

1: Input: Initial parameters  $\theta_{\text{org}}$ , learning rate  $\text{lr}$ , number of iterations  $T$ , and hyperparameters  $\gamma, \tau$ .
2: Initialize the moving-average retention gradient:  $\bar{\mathbf{g}}_r^{(0)} \leftarrow \mathbf{0}$ .
3: for  $t = 0, 1, \dots, T - 1$  do
4:   // 1) Sample a mini-batch from the unlearning dataset  $\mathcal{D}_u$ .
5:    $\mathcal{B}_u^{(t)} \subset \mathcal{D}_u$ .
6:   // 2) Sample a mini-batch from the retention dataset  $\mathcal{D}_r$ .
7:    $\mathcal{B}_r^{(t)} \subset \mathcal{D}_r$ .
8:   // 3) Compute the unlearning gradient  $\mathbf{g}_u$ .
9:    $\mathbf{g}_u^{(t)} \leftarrow \nabla_{\theta} \mathcal{L}(\mathcal{B}_u^{(t)}; \theta^{(t)})$ .
10:  // 4) Compute the retention gradient  $\mathbf{g}_r$ .
11:   $\mathbf{g}_r^{(t)} \leftarrow \nabla_{\theta} \mathcal{R}_r(\mathcal{B}_r^{(t)}; \theta^{(t)})$ .
12:  // 5) Apply exponential moving average to stabilize the retention gradient.
13:   $\bar{\mathbf{g}}_r^{(t)} \leftarrow (1 - \gamma)\bar{\mathbf{g}}_r^{(t-1)} + \gamma\mathbf{g}_r^{(t)}$ .
14:  // 6) Check whether gradients conflict: if the dot product is negative, project out the conflicting component.
15:  if  $\langle \mathbf{g}_u^{(t)}, \bar{\mathbf{g}}_r^{(t)} \rangle < 0$  then
16:     $\tilde{\mathbf{g}}_u^{(t)} \leftarrow \mathbf{g}_u^{(t)} - \frac{\langle \mathbf{g}_u^{(t)}, \bar{\mathbf{g}}_r^{(t)} \rangle}{\|\bar{\mathbf{g}}_r^{(t)}\|^2} \bar{\mathbf{g}}_r^{(t)}$ .
17:  else
18:     $\tilde{\mathbf{g}}_u^{(t)} \leftarrow \mathbf{g}_u^{(t)}$ .
19:  end if
20:  // 7) Optionally clip the rectified gradient norm to avoid overly large updates.
21:  if  $\|\tilde{\mathbf{g}}_u^{(t)}\| > \tau$  then
22:     $\tilde{\mathbf{g}}_u^{(t)} \leftarrow \tau \frac{\tilde{\mathbf{g}}_u^{(t)}}{\|\tilde{\mathbf{g}}_u^{(t)}\|}$ .
23:  end if
24:  // 8) Update the parameters using the rectified gradient.
25:   $\theta^{(t+1)} \leftarrow \theta^{(t)} - \text{lr}^{(t)} \tilde{\mathbf{g}}_u^{(t)}$ ;
26: end for
27: Return  $\theta^{(T)}$ .

```

---

projected in the direction that is orthogonal to  $\bar{\mathbf{g}}_r^{(t)}$ . Please refer to Figure 3 for some visual illustrations. Moreover, we present the implementation of our GRU in Algorithm 1, further elaborating on several key details as follows.

**Stable Estimation.** In practice, we typically utilize stochastic mini-batches of data to estimate the exact values of  $\mathbf{g}_r^{(t)}$  outlined in Eq. (7), which may lead to stochastic errors especially when the batch size is small, often the cases for LLM unlearning. Therefore, we employ the exponential moving average (EMA) to mitigate the additional computation costs associated with increasing batch sizes, namely,

$$\bar{\mathbf{g}}_r^{(t)} = (1 - \gamma)\bar{\mathbf{g}}_r^{(t-1)} + \gamma\mathbf{g}_r^{(t)}, \quad (9)$$

where  $\gamma \in [0, 1)$  is the smoothing parameter, of which smaller values suggest that a broader range of recent batches is covered, indicating a large batch size implicitly. It is worth noting that EMA is an approximation of using large batch sizes, given that  $\theta$  itself is also updated throughout the steps  $t$ . Therefore, selecting the appropriate value for  $\gamma$  is crucial, as it involves balancing the representation of a larger batch size against minimizing the induced errors.

**Gradient Clipping.** Due to stochastic variations and low-order approximations, the rectified gradients may inadvertently encroach upon regions that may decrease retention. To further enhance the practical reliability of our GRU, we further constrain the gradient norm via gradient clipping, following many previous works such as [16, 26]. Specifically, the gradients are scaled down to ensure it stays within a bounded range, i.e.,

$$\tilde{\mathbf{g}}_u^{(t)} \leftarrow \begin{cases} \tilde{\mathbf{g}}_u^{(t)}, & \text{if } \|\tilde{\mathbf{g}}_u^{(t)}\| \leq \tau \\ \tau \tilde{\mathbf{g}}_u^{(t)} / \|\tilde{\mathbf{g}}_u^{(t)}\|, & \text{if } \|\tilde{\mathbf{g}}_u^{(t)}\| > \tau \end{cases}, \quad (10)$$

where  $\tau$  is the predefined threshold for the maximal-allowed value for the norm of the rectified gradients.

### 3.3 Theoretical Analysis

In this section, we present formal analyses to further substantiate the efficacy of our GRU, which focuses on two main aspects: **a) Efficacy in Removal:** In Theorem 3.1, we demonstrate the convergence of the GRU updating dynamics for unlearning. **b) Reliability in Retention:** In Theorem 3.3, we illustrate that our GRU is capable to preserve overall model performance, surpassing the cases without GRU. Overall, we formally verify that our GRU can mitigate the notorious trade-off between removal and retention, thus ensuring overall superior unlearning efficacy.

We begin by showing that unlearning with GRU ensures convergence in line with the original objective of unlearning.

**Theorem 3.1.** *Assume the unlearning objective  $\mathcal{L}$  is differentiable,  $L$ -smooth, and lower bounded. Then, the GRU update rule with the learning rate  $\iota r < 2/L$  will converge to either **a)** a degenerate configuration where  $\cos(\mathbf{g}_u^{(t)}, \mathbf{g}_r^{(t)}) = -1$  at a specific step  $t$ , or **b)** the locally optimal solution  $\theta^*$  that minimizes  $\mathcal{L}(\mathcal{D}_u; \theta)$ .*

*Remark 3.2.* Overall, Theorem 3.1 demonstrates that, from a convergence perspective, the GRU does not compromise the original goal of unlearning. This is contingent upon avoiding those cases where  $\cos(\mathbf{g}_u^{(t)}, \mathbf{g}_r^{(t)}) = -1$ . Moreover, since stochastic optimization is employed for the LLM unlearning process, we can simply overcome this issue by randomly selecting a new data batch from the unlearning dataset, which will then allow the unlearning process to continue to be carried out. Please refer to Appendix A.2 for the detailed proof.

Moreover, central to our motivation, we justify that our GRU can better maintain model performance on non-targeted data compared to original unlearning rules without GRU.

**Theorem 3.3.** *Assume that the retain loss  $\mathcal{R}$  is differentiable and  $L$ -smooth, and the  $\iota r$ -curvature  $\mathfrak{H}_{\iota r}(\mathcal{R}; \mathbf{g})$  for  $\mathcal{R}$  (cf. Definition A.1) satisfies  $\mathfrak{H}_{\iota r}(\mathcal{R}; \mathbf{g}) \geq \ell \|\mathbf{g}\|^2$  for any gradients  $\mathbf{g}$  and some constant  $\ell \leq L$ . Let  $\theta_{\text{gru}}^{(t+1)}$  and  $\theta_u^{(t+1)}$  be the parameters after applying one step of gradient updates for the original  $\theta^{(t)}$  with and without GRU, respectively. Then, we can ensure  $\mathcal{R}(\mathcal{D}_r; \theta_{\text{gru}}^{(t+1)}) \leq \mathcal{R}(\mathcal{D}_r; \theta_u^{(t+1)})$  if **a)**  $\ell \geq \frac{\|\mathbf{g}_u^{(t)} - \mathbf{g}_r^{(t)}\|^2}{\|\mathbf{g}_u^{(t)} + \mathbf{g}_r^{(t)}\|^2} L$  and **b)**  $\ell \geq \frac{\|\mathbf{g}_u^{(t)} - \mathbf{g}_r^{(t)}\|^2}{\|\mathbf{g}_u^{(t)} + \mathbf{g}_r^{(t)}\|^2} L + 2/\iota r$ .*

*Remark 3.4.* In heuristics,  $\frac{\|\mathbf{g}_u^{(t)} - \mathbf{g}_r^{(t)}\|^2}{\|\mathbf{g}_u^{(t)} + \mathbf{g}_r^{(t)}\|^2}$  measures the degree of conflict between  $\mathbf{g}_u^{(t)}$  and  $\mathbf{g}_r^{(t)}$ , of which the larger values generally indicate a greater destructive effect on the retain performance. Therefore, condition **a)** implies that when the degree of conflict is more severe, our requirements for models, characterized by  $\ell/L$ , will also be more stringent; condition **b)** states that to ensure the overall efficacy of our proposed method in terms of retention, the learning rate adopted in GRU should not be excessively small. Please refer to Appendix A.3 for the detailed proof.

Overall, Theorem 3.1 ensures that GRU will not compromise convergence for the original unlearning objective, and Theorem 3.3 further characterizes its behaviors in preserving the overall model performance. Taken together, we certify the efficacy of our GRU in mitigating the notorious trade-off between removal and retention.

## 4 Go Beyond GRU

Most unlearning methods, including our GRU, rely on retain data to preserve the overall performance. However, retain data can often be biased, motivating us to investigate a challenging scenario where we need to rely exclusively on the unlearn data  $\mathcal{D}_u$ , without further access to the retain data  $\mathcal{D}_r$ . To adapt for this setup, we make several adjustments for GRU and propose **task vector rectified unlearning (TRU)**.

The key insight behind TRU is that unlearning typically involves a series of data points rather than a single instance. Thus, for each individual data point  $s_u \in \mathcal{D}_u$  targeted for unlearning, the remaining data points within  $\mathcal{D}_u$ , i.e.,  $\mathcal{D}_u \setminus \{s_u\}$ , can offer information for retention if used properly. Here, we incorporate the so-called task vectors [27], which are as the essential component of our algorithmic design, into our process.

**Task Vector.** A task vector typically represents the necessary adjustments for model parameters to incorporate new knowledge. For example, when we want the model to learn from a specific data point  $s$ , we initiate by fine-tuning the current model parameterized, denoted by  $\theta_{\text{org}}$ . It can be achieved through  $T$  iterations of gradient updates, following  $\theta^{(t+1)} = \theta^{(t)} + \iota r \cdot \nabla_{\theta} \log p(s; \theta^{(t)})$  with  $\theta^{(0)} = \theta_{\text{org}}$  and  $\theta_s = \theta^{(T)}$ . Obviously,  $T_s$  allows for the augmentation of the original model with the knowledge acquired from  $s$  by applying  $\theta_{\text{org}} + T_s$ . Conversely, to unlearn a data point  $s_u$ , we can reverse this process by subtracting the task vector via  $\theta_{\text{org}} - T_{s_u}$  [28].

**Rectified Task Vector.** However, the task vector  $\mathbf{T}_{s_u}$  still faces the trade-off between unlearning and retention. Hence, a similar constrained updating rule, as outlined in Eq. (7), can be adopted and further adjusted as:

$$\begin{aligned} \min_{\tilde{\mathbf{T}}_{s_u}} \quad & \|\tilde{\mathbf{T}}_{s_u} - \mathbf{T}_{s_u}\|^2 \\ \text{s.t.} \quad & \langle -\tilde{\mathbf{T}}_{s_u}, \nabla_{\theta} \mathcal{R}(\mathcal{D}_u \setminus \{s_u\}; \theta_{\text{org}}) \rangle \geq 0. \end{aligned} \quad (11)$$

It mandates that the task vectors be rectified to have no negative impact on other data points. For this purpose, we utilize other unlearning data, i.e.,  $\mathcal{D}_u \setminus \{s_u\}$ , as reference. Similar to Eq. (8), we have its closed-form solution as

$$\tilde{\mathbf{T}}_{s_u} = \mathbf{T}_{s_u} + \frac{[\langle \mathbf{T}_{s_u}, \nabla_{\theta} \mathcal{R}(\mathcal{D}_u \setminus \{s_u\}; \theta_{\text{org}}) \rangle]_-}{\|\nabla_{\theta} \mathcal{R}(\mathcal{D}_u \setminus \{s_u\}; \theta_{\text{org}})\|^2} \mathbf{T}_{s_u}. \quad (12)$$

For each data point  $s_u$  within  $\mathcal{D}_u$ , we can calculate the associated task vector  $\tilde{\mathbf{T}}_{s_u}$ . Moreover, to ensure standardised influence across data points, these task vectors are further normalized so that their magnitudes are equal to 1. The resulting normalized vectors are denoted as  $\bar{\mathbf{T}}_{s_u}$ , facilitating equitable integration across data points, as shown below.

To unlearn the entire set  $\mathcal{D}_u$ , we subtract the average of all normalized task vectors from the original model. This is implemented using the formula of

$$\theta_{\text{org}} - \frac{\text{stg}}{n} \sum_{s_u \in \mathcal{D}_u} \bar{\mathbf{T}}_{s_u}, \quad (13)$$

where  $n$  represents the number of data points within  $\mathcal{D}_u$  and  $\text{stg}$  indicates the strength of task vector-based unlearning. It ensures a reliable removal of targeted data, meanwhile mitigating the compromise to the overall performance. Moreover, when the number of data points  $n$  is substantial, an effective strategy involves randomly dividing the entire unlearning set into several smaller batches. Each batch then serves as a substitute for  $s_u$  in Eq. (11), reducing the demands associated with calculating the task vectors.

## 5 Experiments

In this section, we conduct extensive experiments to verify the effectiveness of our GRU in mitigating the trade-off involved in LLM unlearning. To begin with, we first offer a brief description of our experimental setups.

**Benchmarks.** Our evaluations adopt three representative benchmarks: TOFU [14], WMDP [18], and MUSE [19]. TOFU comprises 200 synthetic author profiles, a total of 4,000 question-answer pairs. It covers different unlearning setups with varying proportions of data targeted to be unlearned, including 1%, 5%, or 10% of the profiles as unlearning sets. WMDP collects a set of sensitive knowledge encountered in practice, further categorized into three areas as biosecurity, cybersecurity, and chemical security. MUSE constructs their unlearning sets using news articles and books, primarily focusing on addressing copyright issues within existing LLMs.

**Baselines and Backbones.** For the baseline methods, we focus on a set of objective-based approaches, including GA, GD, NPO, and weighted gradient ascent (WGA) [24]. All of these methods have demonstrated their practical significance and are thus adopted in our experiments. Moreover, for the backbone models, we adhere to the default suggestions for each benchmark. We use further fine-tuned LLaMA2-7B-chat [29] and Phi-1.5 [30] for TOFU; Zephyr-7B-beta [31] for WMDP; ICLM-7B [32] for MUSE.

**Hyper-parameters Configurations.** In our experiments, we use AdamW optimizer [33] with a batch size of 32 and learning rates  $2 \times 10^{-5}$  for Phi-1.5 and  $1 \times 10^{-5}$  for LLaMA2-7B-chat in TOFU;  $1 \times 10^{-5}$  in MUSE;  $4 \times 10^{-6}$  in WMDP. Furthermore, the training steps are set to 5 epochs for TOFU, 1 epoch for MUSE, and 20 steps for WMDP. For hyperparameters in GRU, we employ grid search on validation data to identify their optimal values. The candidate values for  $\gamma$  include  $\{0.01, 0.05, 0.1, 0.2, 0.3, 0.4, 0.5, 0.6, 0.7, 0.8, 0.9, 0.99\}$ , and for  $\tau$  are  $\{0.001, 0.005, 0.01, 0.1, 1.0, 10, 100\}$ . Their specific choices and impacts across different baseline methods are detailed in Appendix C.

**Metrics.** We adhere to the suggested evaluation metrics for each benchmark. TOFU adopts two metrics: FQ and MU. FQ measures the extent of data removal by the statistical difference in responses between unlearned models and ground-standard models, which are trained without targeted data. Higher values of FQ are preferred and we report the logarithm of the original FQ values for enhanced readability. MU assesses the overall performance of retention, which is a combination of several more foundational metrics. It can be computed on the retain sets, real authors, and world facts, where higher values indicate better retention.

WMDP performs QA evaluations on WMDP-Bio and WMDP-Cyber to assess the efficacy of removal, where the prompts are standardized following [34]. For retention, WMDP also utilizes QA evaluations but conducted on the MMLU benchmark. Therein, smaller values of QA evaluations are preferred for WMDP-Bio and WMDP-Cyber,

## Mitigating the Trade-off between Unlearning and Retention for LLMs

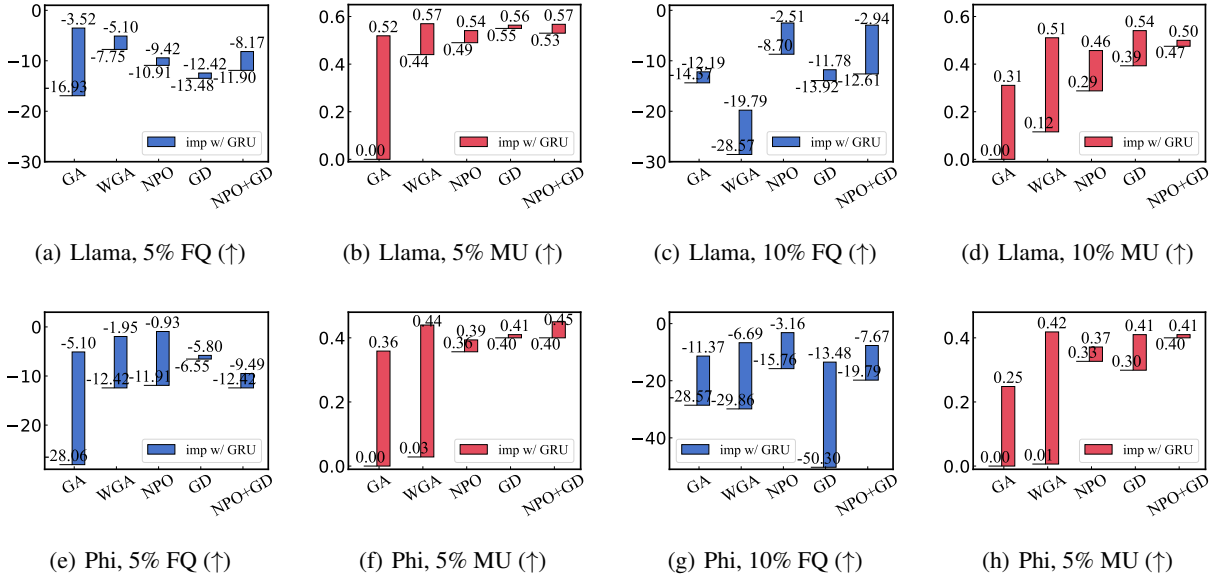


Figure 4: Experimental results on the TOFU benchmarks: Evaluating 5% and 10% unlearning setups using Llama-2-7B (Llama) and Phi-1.5 (Phi) backbones. We present metric scores—either FQ or MU—both without and with GRU, displayed in pairs and highlighted the corresponding improvements after GRU (imp w/ GRU) with colored bars. For example, in (a), the FQ values of -16.93 (w/o GRU) and -3.52 (w/ GRU) for GA are connected by a blue-colored bar, signifying the improvements attributed to GRU.

while larger values are desired for MMLU. Moreover, MUSE proposes two metrics to assess the removal efficacy, i.e., VerbMem and KnowMem, quantifying various aspects of memorization and membership inference.

MUSE also uses KnowMem for assessing performance retention, where larger values are preferred. To ease analysis, we use the symbols  $\uparrow$  and  $\downarrow$  next to metric names to indicate that their larger/smaller values are preferred.

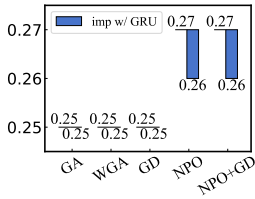
**Hardware Configurations.** All our experiments are conducted with a series of computation nodes powered by NVIDIA-A100-80GB GPUs and Intel(R) Xeon(R) Gold 6248R CPUs. All our codes are implemented on Transformers version 4.42.4 and CUDA version 12.1.

### 5.1 Main Results

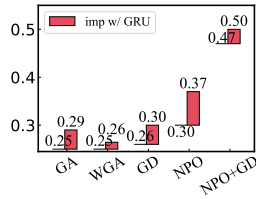
GRU is a general framework compatible with a wide range of objective-based unlearning methods. In this section, we demonstrate its reliability by integrating it with various unlearning approaches. Our goal is to show the universal improvements achieved with GRU across different methods in both removal and retention, thereby justifying the overall efficacy of our GRU in mitigating their trade-off.

**TOFU Benchmark.** We consider five representative baseline methods—GA, WGA, NPO, GD, and NPO+GD—to validate their performance improvements after implementing GRU in terms of both removal (FQ) and retention (MU) metrics. We summarize our experimental results in Figure 4, focusing on the challenging setups of 5% and 10% unlearning. Additional experimental setups and baseline methods are detailed in Appendix B. We observe uniform improvements in both FQ and MU metrics after applying GRU, across various methods, unlearning setups, and backbone models. Surprisingly, even for methods typically viewed as less promising, such as GA, we observe significant enhancements in both removal and retention after incorporating GRU. The improvements observed in other methods, such as WGA and GD, are also very impressive.

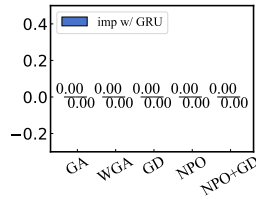
On the other side, with the integration of GRU, it remains difficult to identify a single baseline method that always outperforms others across different unlearning scenarios and setups. For example, with Phi-1.5, WGA and NPO are more effective than others. When coming to Llama-2-7B, GA and WGA tend to be more suitable under the 5% unlearning setup, whereas NPO and NPO+GD show greater efficacy under a 10% unlearning setup. Thus, while GRU uniformly enhances the overall efficacy of unlearning, the selection of baseline methods remains a task-dependent consideration that requires careful selection.



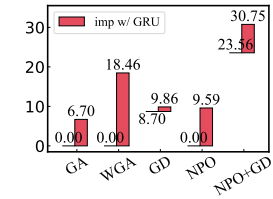
(a) Bio Unlearning (↓)



(b) MMLU Retention (↑)



(a) KnowMem-U (↓)



(b) KnowMem-R (↑)

Figure 5: Experimental results on the WMDP benchmarks with QA accuracies on Bio unlearning and MMLU, quantifying the efficacy of removal and retention, respectively.

Figure 6: Experimental results on the MUSE benchmarks with KnowMem, assessing the efficacy of removal and retention on targeted and non-targeted data, respectively.

Table 1: Experimental results on the TOFU benchmarks within the retain-data-free settings are presented. We compare our TRU with representative baseline models, across different unlearning setups and backbone architectures. The top-performing results in each column are highlighted in bold to ease reference.

Method	Phi-1.5				Llama2-7B			
	5%		10%		5%		10%	
	FQ↑	MU↑	FQ↑	MU↑	FQ↑	MU↑	FQ↑	MU↑
original	-28.84	0.52	-40.52	0.52	-32.13	0.63	-48.59	0.63
retrain	0.00	0.52	0.00	0.53	0.00	0.60	0.00	0.61
TV	-46.18	0.00	-36.06	0.00	-22.13	0.00	-9.06	0.00
GA	-28.06	0.00	-28.57	0.00	-16.93	0.00	-14.37	0.00
WGA	-12.42	0.03	-29.86	0.01	-7.75	0.44	-28.57	0.12
NPO	-11.91	0.36	-15.76	0.33	-10.91	0.49	-8.70	0.29
TRU	<b>-9.04</b>	<b>0.40</b>	<b>-13.04</b>	<b>0.36</b>	<b>-7.34</b>	<b>0.53</b>	<b>-4.92</b>	<b>0.47</b>

**WMDP and MUSE Benchmarks.** To further substantiate the general efficacy and reliability of our GRU, we conduct additional experiments using the WMDP and MUSE benchmarks, of which the results are detailed in Figure 5 and Figure 6, respectively. Note that the minimum values for QA accuracy and KnowMem are 0.25 and 0, and thus the results shown for GA and GD in Figure 5(a) and for all methods in Figure 6 cannot decrease further.

Overall, our results demonstrate that GRU remains reliable across various baseline methods and unlearning setups, enhancing the overall efficacy of unlearning with notable improvements or maintenance in both the goals of data removal and retention. Additionally, it is evident that the NPO-based methods generally deliver superior performance. Given these observations, which can be recommended as our default choices for effective unlearning.

## 5.2 Retain Data Free

We further consider the retain-data-free settings, where we have no retain data at hand as mentioned in Section 4. As a case study, we test the efficacy of various methods that do not rely on retain data and our TRU. We further include the baseline of task vector (TV) [27] for fair comparison, which is also the key technique that is adopted in our TRU. The experimental results are summarized in Table 1, where we also report metric scores for the model before unlearning (original) as well as for the gold standard model (retrain), which is fine-tuned from scratch without the targeted data. Across baseline methods, it can be observed that the retain-data-free settings is challenging. Only WGA and NPO can demonstrate some ability of reliable unlearning. In contrast, other methods, such as TV and GA, can render the unlearned models completely useless. Furthermore, our TRU exhibits notable improvements over these baselines in both removal and retention, showcasing the broad applications of our unlearning schemes suggested in Eq. (7) even in some more restricted unlearning setups.

Table 2: Hyper-parameter turning of  $\tau$  on TOFU with Llama-2-7B, under the 5% unlearning setup.

Method	Metric	$\tau$								
		0.001	0.01	0.1	1.0	2.0	3.0	10	100	N/A
GA w/ GRU	FQ $\uparrow$	-29.6514	-15.7370	-7.7503	-8.6008	-4.7631	-4.4360	-2.9534	-3.2299	-3.5161
	MU $\uparrow$	0.6326	0.5824	0.5761	0.5810	0.5684	0.5550	0.5121	0.5149	0.5190
NPO w/ GRU	FQ $\uparrow$	-27.2750	-18.7967	-12.9485	-9.0417	-9.4931	-9.9550	-9.9550	-10.4275	-9.9550
	MU $\uparrow$	0.6268	0.5796	0.5574	0.5220	0.5519	0.5318	0.5312	0.5373	0.5408
GD w/ GRU	FQ $\uparrow$	-27.2750	-18.7967	14.0316	-15.1577	-14.5893	-14.5893	-15.7370	-12.4230	-12.4230
	MU $\uparrow$	0.6200	0.5395	0.5442	0.5434	0.5467	0.5467	0.5484	0.5637	0.5637

### 5.3 Sensitivity Analyses

As a case study, we conduct sensitivity analyses on TOFU with Llama-2-7B as the backbone, under the 5% unlearning setup.

**Gradient Clipping.** We first present the results across various values of  $\tau$ , summarized in Table 2. The results show that, across different baselines, the effects of altering  $\tau$  have a smooth control over the performance metrics of FQ and MU. This observation indicates that our GRU exhibits robustness with respect to different choices of  $\tau$ .

**Exponential Moving Average.** We further display the results across different  $\gamma$  in Table 3. As with the gradient clipping, we observe a smooth control on the overall efficacy of unlearning, further indicating that our GRU method demonstrates robustness against variations in its two hyper-parameters.

**Unlearning Strength.** We also report a range of strength  $\text{stg}$  in Table 4 for our task vector-based unlearning approach. The observed numerical stability in both unlearning and retention performance underscores the robust efficacy of our proposed ‘‘rectification’’ framework.

Table 3: Hyper-parameter turning of  $\gamma$  on TOFU with Llama-2-7B, under the 5% unlearning setup. The notation ‘‘-’’ indicates that the associated result is same to those without GRU.

Method	Metric	$\gamma$												
		0.01	0.02	0.05	0.1	0.2	0.3	0.4	0.5	0.6	0.8	0.9	0.99	N/A
GA w/ GRU	FQ $\uparrow$	-6.9414	-5.8059	-6.9414	-7.3407	-8.1703	-7.3407	-6.5526	-7.7503	-6.5526	-8.6008	-6.5526	-8.6008	-8.1703
	MU $\uparrow$	0.4528	0.4418	0.4715	0.4994	0.5247	0.5504	0.5601	0.5677	0.5739	0.5810	0.5827	0.5847	0.5829
NPO w/ GRU	FQ $\uparrow$	-11.9082	-11.4040	-9.9550	-9.9550	-9.4931	-8.6008	-8.1703	-9.0417	-9.0417	-9.0417	-10.4275	-10.9105	-9.0417
	MU $\uparrow$	0.4736	0.4773	0.4865	0.4952	0.5108	0.5144	0.5159	0.5178	0.5222	0.5220	0.5425	0.5358	0.5656
GD w/ GRU	FQ $\uparrow$	-12.9485	-12.4230	-12.4230	-14.0316	-12.9485	-11.9082	-14.0316	-14.0316	-13.4847	-	-	-	-
	MU $\uparrow$	0.5642	0.5640	0.5637	0.5615	0.5604	0.5585	0.5586	0.5592	0.5582	-	-	-	-

### 5.4 Ablation Studies.

Previous works, such as [15], also use gradient clipping (GC) to improve the overall efficacy of unlearning, raising us to ask if our rectification mechanism plays a key role in mitigating the trade-off between removal and retention. In Table 5, we conduct ablation studies on TOFU using Llama-2-7B as the backbone, focusing on the 5% unlearning setup. We compare three scenarios: the original unlearning method without GRU (w/o GRU), the original method enhanced with GC (w/ GC), and the unlearning method that incorporates GRU (w/ GRU). As evident from the results, GRU demonstrates superior scores in terms of both FQ and MU, showing its efficacy in mitigating the trade-off between removal and retention.

### 5.5 More Results in Appendices

Due to space limits, we leave more detailed experimental results and additional analyses in the appendices. For convenience, this section provides a brief overview of these contents: In Appendix B, we offer more comprehensive results for our main experiments on varying benchmarks and metrics, further covering other baselines such as SimNPO [35] and NPO+KL. In Appendix C, we detail the hyper-parameter configurations and outline their recommended setups. Finally, in Appendix D, we include other experimental analyses of GRU.

Table 4: Hyper-parameter turning of RDF on the TOFU-llama-%5 with different Task Vector strength  $stg$ .

Metric	stg							
	0.50	0.55	0.60	0.65	0.70	0.75	0.80	0.85
FQ $\uparrow$	-9.9550	-7.3407	-6.5526	-4.4360	-2.4323	-1.7263	-0.6065	-0.3389
MU $\uparrow$	0.5509	0.5251	0.4856	0.4507	0.4211	0.3812	0.3526	0.3233

Table 5: Ablation studies on TOFU with Llama-2-7B, under the 5% unlearning setup.

Method	Component	FQ $\uparrow$	MU $\uparrow$
GA	w/o GRU	-16.9281	0.0000
	w/ GC	-20.7646	0.0000
	w/ GRU	<b>-3.2299</b>	<b>0.5149</b>
NPO	w/o GRU	-10.9105	0.4919
	w/ GC	-10.9105	0.4970
	w/ GRU	<b>-10.4275</b>	<b>0.5373</b>

## 6 Conclusion

This paper introduces GRU, a novel and general framework designed to mitigate the inherent trade-off between data removal and retention for LLM unlearning, a critical challenge in this field. Our key insight involves regulating the gradients used for unlearning by projecting them onto the orthogonal complement of directions that negatively affect retention. Thereby, GRU ensures that the unlearning updates minimize their adverse impact on the overall model performance. We offer both theoretical analyses and empirical evidence to demonstrate the effectiveness of our method in mitigating the trade-off between removal and retention, resulting in the overall efficacy of unlearning. However, our method critically relies on the quality of retain data. While TRU can mitigate this issue to some extent, potential biases and distribution shifts therein may still be detrimental. In the future, we will explore ways to pursue reliable LLM unlearning without relying on retain data or their surrogates.

## Impact Statements

This work has notable societal implications by spurring the development of LLMs that meet both ethical and legal standards, thus mitigating the risks of privacy breaches and the unauthorized spread of protected information. We advocate for continued research into legally sound and reliable LLMs that honor individual rights and intellectual property while maintaining their robustness across numerous applications. By paving the way for broader deployment of LLMs capable of adapting to evolving legal and ethical requirements, this line of work helps ensure that the broader adoption of LLMs that can adapt to evolving legal and ethical standards remains both trustworthy and socially beneficial.

## References

- [1] Hugo Touvron, Thibaut Lavril, Gautier Izacard, Xavier Martinet, Marie-Anne Lachaux, Timothée Lacroix, Baptiste Rozière, Naman Goyal, Eric Hambro, Faisal Azhar, et al. Llama: Open and efficient foundation language models. *arXiv preprint arXiv:2302.13971*, 2023.
- [2] Josh Achiam, Steven Adler, Sandhini Agarwal, Lama Ahmad, Ilge Akkaya, Florencia Leoni Aleman, Diogo Almeida, Janko Altenschmidt, Sam Altman, Shyamal Anadkat, et al. Gpt-4 technical report. *arXiv preprint arXiv:2303.08774*, 2023.
- [3] Tom Brown, Benjamin Mann, Nick Ryder, Melanie Subbiah, Jared D Kaplan, Prafulla Dhariwal, Arvind Nee-lakantan, Pranav Shyam, Girish Sastry, Amanda Askell, et al. Language models are few-shot learners. In *NeurIPS*, 2020.

- [4] Zhangir Azerbayev, Hailey Schoelkopf, Keiran Paster, Marco Dos Santos, Stephen McAleer, Albert Q Jiang, Jia Deng, Stella Biderman, and Sean Welleck. Llemma: An open language model for mathematics. *arXiv preprint arXiv:2310.10631*, 2023.
- [5] Baptiste Roziere, Jonas Gehring, Fabian Gloeckle, Sten Sootla, Itai Gat, Xiaoqing Ellen Tan, Yossi Adi, Jingyu Liu, Tal Remez, Jérémy Rapin, et al. Code llama: Open foundation models for code. *arXiv preprint arXiv:2308.12950*, 2023.
- [6] Shijie Wu, Ozan Irsoy, Steven Lu, Vadim Dabravolski, Mark Dredze, Sebastian Gehrmann, Prabhajan Kambadur, David Rosenberg, and Gideon Mann. Bloomberggpt: A large language model for finance. *arXiv preprint arXiv:2303.17564*, 2023.
- [7] Arun James Thirunavukarasu, Darren Shu Jeng Ting, Kabilan Elangovan, Laura Gutierrez, Ting Fang Tan, and Daniel Shu Wei Ting. Large language models in medicine. *Nature medicine*, 29(8):1930–1940, 2023.
- [8] Fabio Petroni, Tim Rocktäschel, Patrick Lewis, Anton Bakhtin, Yuxiang Wu, Alexander H Miller, and Sebastian Riedel. Language models as knowledge bases? *arXiv preprint arXiv:1909.01066*, 2019.
- [9] Nora Belrose, Zach Furman, Logan Smith, Danny Halawi, Igor Ostrovsky, Lev McKinney, Stella Biderman, and Jacob Steinhardt. Eliciting latent predictions from transformers with the tuned lens. *arXiv preprint arXiv:2303.08112*, 2023.
- [10] Yifan Yao, Jinhao Duan, Kaidi Xu, Yuanfang Cai, Eric Sun, and Yue Zhang. A survey on large language model (llm) security and privacy: The good, the bad, and the ugly. *arXiv preprint arXiv:2312.02003*, 2023.
- [11] Sijia Liu, Yuanshun Yao, Jinghan Jia, Stephen Casper, Nathalie Baracaldo, Peter Hase, Xiaojun Xu, Yuguang Yao, Hang Li, Kush R Varshney, et al. Rethinking machine unlearning for large language models. *arXiv preprint arXiv:2402.08787*, 2024.
- [12] Dawen Zhang, Pamela Finckenberg-Broman, Thong Hoang, Shidong Pan, Zhenchang Xing, Mark Staples, and Xiwei Xu. Right to be forgotten in the era of large language models: Implications, challenges, and solutions. *arXiv preprint arXiv:2307.03941*, 2023.
- [13] Yuanshun Yao, Xiaojun Xu, and Yang Liu. Large language model unlearning. *arXiv preprint arXiv:2310.10683*, 2023.
- [14] Pratyush Maini, Zhili Feng, Avi Schwarzschild, Zachary C Lipton, and J Zico Kolter. Tofu: A task of fictitious unlearning for llms. *arXiv preprint arXiv:2401.06121*, 2024.
- [15] Ruiqi Zhang, Licong Lin, Yu Bai, and Song Mei. Negative preference optimization: From catastrophic collapse to effective unlearning. *arXiv preprint arXiv:2404.05868*, 2024.
- [16] Qizhou Wang, Bo Han, Puning Yang, Jianing Zhu, Tongliang Liu, and Masashi Sugiyama. Unlearning with control: Assessing real-world utility for large language model unlearning. *arXiv preprint arXiv:2406.09179*, 2024.
- [17] Nicholas Carlini, Florian Tramer, Eric Wallace, Matthew Jagielski, Ariel Herbert-Voss, Katherine Lee, Adam Roberts, Tom Brown, Dawn Song, Ulfar Erlingsson, et al. Extracting training data from large language models. In *USENIX Security*, 2021.
- [18] Nathaniel Li, Alexander Pan, Anjali Gopal, Summer Yue, Daniel Berrios, Alice Gatti, Justin D Li, Ann-Kathrin Dombrowski, Shashwat Goel, Long Phan, et al. The wmdp benchmark: Measuring and reducing malicious use with unlearning. *arXiv preprint arXiv:2403.03218*, 2024.
- [19] Weijia Shi, Jaechan Lee, Yangsibo Huang, Sadhika Malladi, Jieyu Zhao, Ari Holtzman, Daogao Liu, Luke Zettlemoyer, Noah A Smith, and Chiyuan Zhang. Muse: Machine unlearning six-way evaluation for language models. *arXiv preprint arXiv:2407.06460*, 2024.
- [20] Wayne Xin Zhao, Kun Zhou, Junyi Li, Tianyi Tang, Xiaolei Wang, Yupeng Hou, Yingqian Min, Beichen Zhang, Junjie Zhang, Zican Dong, et al. A survey of large language models. *arXiv preprint arXiv:2303.18223*, 2023.
- [21] Badhan Chandra Das, M Hadi Amini, and Yanzhao Wu. Security and privacy challenges of large language models: A survey. *arXiv preprint arXiv:2402.00888*, 2024.
- [22] Ronen Eldan and Mark Russinovich. Who’s harry potter? approximate unlearning in llms. *arXiv preprint arXiv:2310.02238*, 2023.

- [23] Yifan Yao, Jinhao Duan, Kaidi Xu, Yuanfang Cai, Zhibo Sun, and Yue Zhang. A survey on large language model (llm) security and privacy: The good, the bad, and the ugly. *High-Confidence Computing*, page 100211, 2024.
- [24] Qizhou Wang, Jin Peng Zhou, Zhanke Zhou, Saebyeol Shin, Bo Han, and Kilian Q Weinberger. Rethinking llm unlearning objectives: A gradient perspective and go beyond. *arXiv preprint arXiv:2406.09179*, 2024.
- [25] Rafael Rafailov, Archit Sharma, Eric Mitchell, Christopher D Manning, Stefano Ermon, and Chelsea Finn. Direct preference optimization: Your language model is secretly a reward model. In *NeurIPS*, 2024.
- [26] Mitchell Wortsman, Gabriel Ilharco, Jong Wook Kim, Mike Li, Simon Kornblith, Rebecca Roelofs, Raphael Gontijo Lopes, Hannaneh Hajishirzi, Ali Farhadi, Hongseok Namkoong, et al. Robust fine-tuning of zero-shot models. In *CVPR*, 2022.
- [27] Gabriel Ilharco, Marco Tulio Ribeiro, Mitchell Wortsman, Suchin Gururangan, Ludwig Schmidt, Hannaneh Hajishirzi, and Ali Farhadi. Editing models with task arithmetic. *arXiv preprint arXiv:2212.04089*, 2022.
- [28] George-Octavian Barbulescu and Peter Triantafillou. To each (textual sequence) its own: Improving memorized-data unlearning in large language models. *arXiv preprint arXiv:2405.03097*, 2024.
- [29] Hugo Touvron, Louis Martin, Kevin Stone, Peter Albert, Amjad Almahairi, Yasmine Babaei, Nikolay Bashlykov, Soumya Batra, Prajjwal Bhargava, Shruti Bhosale, et al. Llama 2: Open foundation and fine-tuned chat models. *arXiv preprint arXiv:2307.09288*, 2023.
- [30] Marah Abdin, Jyoti Aneja, Hany Awadalla, Ahmed Awadallah, Ammar Ahmad Awan, Nguyen Bach, Amit Bahree, Arash Bakhtiari, Jianmin Bao, Harkirat Behl, et al. Phi-3 technical report: A highly capable language model locally on your phone. *arXiv preprint arXiv:2404.14219*, 2024.
- [31] Lewis Tunstall, Edward Beeching, Nathan Lambert, Nazneen Rajani, Kashif Rasul, Younes Belkada, Shengyi Huang, Leandro von Werra, Clémentine Fourrier, Nathan Habib, et al. Zephyr: Direct distillation of lm alignment. *arXiv preprint arXiv:2310.16944*, 2023.
- [32] Weijia Shi, Sewon Min, Maria Lomeli, Chunting Zhou, Margaret Li, Gergely Szilvassy, Rich James, Xi Victoria Lin, Noah A Smith, Luke Zettlemoyer, et al. In-context pretraining: Language modeling beyond document boundaries. *arXiv preprint arXiv:2310.10638*, 2023.
- [33] Ilya Loshchilov and Frank Hutter. Decoupled weight decay regularization. *arXiv preprint arXiv:1711.05101*, 2017.
- [34] Leo Gao, Jonathan Tow, Baber Abbasi, Stella Biderman, Sid Black, Anthony DiPofi, Charles Foster, Laurence Golding, Jeffrey Hsu, Alain Le Noac’h, Haonan Li, Kyle McDonell, Niklas Muennighoff, Chris Ociepa, Jason Phang, Laria Reynolds, Hailey Schoelkopf, Aviya Skowron, Lintang Sutawika, Eric Tang, Anish Thite, Ben Wang, Kevin Wang, and Andy Zou. A framework for few-shot language model evaluation, 2024.
- [35] Chongyu Fan, Jiancheng Liu, Licong Lin, Jinghan Jia, Ruiqi Zhang, Song Mei, and Sijia Liu. Simplicity prevails: Rethinking negative preference optimization for llm unlearning, 2024.

## A Derivations and Proofs

To begin with, we present our derivations regarding the closed-form solutions for Eq. (7) as well as detailed proofs for theoretical analyses in Section 3.3.

### A.1 The Closed-form Solution of Eq. (7)

Recalling the original optimization problem of

$$\begin{aligned} \arg \min_{\tilde{\mathbf{g}}_u^{(t)}} \quad & \|\tilde{\mathbf{g}}_u^{(t)} - \mathbf{g}_u^{(t)}\|^2 \\ \text{s.t.} \quad & \langle \tilde{\mathbf{g}}_u^{(t)}, \mathbf{g}_r^{(t)} \rangle \geq 0 \end{aligned}$$

We construct the Lagrangian equation following

$$\frac{1}{2} \|\tilde{\mathbf{g}}_u^{(t)} - \mathbf{g}_u^{(t)}\|^2 - \kappa \langle \tilde{\mathbf{g}}_u^{(t)}, \mathbf{g}_r^{(t)} \rangle \quad (14)$$

with  $\kappa \geq 0$  the Lagrange multiplier. Then, setting the gradients Eq. (14) with respect to  $\tilde{\mathbf{g}}_u^{(t)}$  to zero, we have

$$\tilde{\mathbf{g}}_u^{(t)} - \mathbf{g}_u^{(t)} - \kappa \mathbf{g}_r^{(t)} = 0. \quad (15)$$

It indicates that we have the solution of

$$\tilde{\mathbf{g}}_u^{(t)} = \mathbf{g}_u^{(t)} + \kappa \mathbf{g}_r^{(t)}.$$

Substituting it back into the constraint:

$$\langle \tilde{\mathbf{g}}_u^{(t)}, \mathbf{g}_r^{(t)} \rangle = \langle \mathbf{g}_u^{(t)} + \kappa \mathbf{g}_r^{(t)}, \mathbf{g}_r^{(t)} \rangle = \langle \mathbf{g}_u^{(t)}, \mathbf{g}_r^{(t)} \rangle + \kappa \|\mathbf{g}_r^{(t)}\|^2 \geq 0$$

and solving for  $\kappa$ , we have

$$\kappa \geq -\frac{\langle \mathbf{g}_u^{(t)}, \mathbf{g}_r^{(t)} \rangle}{\|\mathbf{g}_r^{(t)}\|^2}.$$

Since  $\kappa \geq 0$ , we can further derive

$$\kappa = \frac{[-\langle \mathbf{g}_u^{(t)}, \mathbf{g}_r^{(t)} \rangle]_+}{\|\mathbf{g}_r^{(t)}\|^2} = \frac{[\langle \mathbf{g}_u^{(t)}, \mathbf{g}_r^{(t)} \rangle]_-}{\|\mathbf{g}_r^{(t)}\|^2}.$$

Then, we can obtain the closed-form for the adjusted gradients as

$$\tilde{\mathbf{g}}_u^{(t)} = \mathbf{g}_u^{(t)} + \frac{[\langle \mathbf{g}_u^{(t)}, \mathbf{g}_r^{(t)} \rangle]_-}{\|\mathbf{g}_r^{(t)}\|^2} \mathbf{g}_r^{(t)}$$

Thus, we complete our derivation for Eq. (7).

We further demonstrate that the GRU causes the magnitudes of the rectified gradients to decrease. To this end, we first decompose the original gradients  $\mathbf{g}_u^{(t)}$  into two orthogonal components that are parallel and perpendicular to  $\mathbf{g}_r^{(t)}$ , which are

$$\mathbf{g}_u^{(t)} = \mathbf{g}_\perp + \mathbf{g}_\parallel \text{ and } \mathbf{g}_\perp \perp \mathbf{g}_r^{(t)}.$$

with  $\mathbf{g}_\parallel$  parallel to  $\mathbf{g}_r^{(t)}$ . In this decomposition,  $\mathbf{g}_\parallel$  represents the component of  $\mathbf{g}_u^{(t)}$  that aligns with  $\mathbf{g}_r^{(t)}$ , whereas  $\mathbf{g}_\perp$  is orthogonal to  $\mathbf{g}_r^{(t)}$ . Then, if  $\langle \mathbf{g}_u^{(t)}, \mathbf{g}_r^{(t)} \rangle \geq 0$ , no adjustment is needed and we keep  $\tilde{\mathbf{g}}_u^{(t)} = \mathbf{g}_u^{(t)}$ . In this case, the norm remains the same as  $\|\tilde{\mathbf{g}}_u^{(t)}\| = \|\mathbf{g}_u^{(t)}\|$ . However, when  $\langle \mathbf{g}_u^{(t)}, \mathbf{g}_r^{(t)} \rangle < 0$ ,  $\mathbf{g}_\parallel$  represents a negatively aligned component with respect to  $\mathbf{g}_r^{(t)}$ . The correction term in Eq. (8) removes this negative parallel portion, thereby setting  $\tilde{\mathbf{g}}_u^{(t)} = \mathbf{g}_\perp$ . Since  $\mathbf{g}_u^{(t)} = \mathbf{g}_\perp + \mathbf{g}_\parallel$ , we have  $\|\mathbf{g}_u^{(t)}\|^2 = \|\mathbf{g}_\perp\|^2 + \|\mathbf{g}_\parallel\|^2$ . When the parallel component is negative relative to  $\mathbf{g}_r^{(t)}$ , its removal decreases the overall norm. Thus, it is easy to conclude that, after rectification, we have

$$\|\tilde{\mathbf{g}}_u^{(t)}\| = \|\mathbf{g}_\perp\| < \|\mathbf{g}_u^{(t)}\|.$$

This difference in magnitudes is influenced by the angles between  $\mathbf{g}_u^{(t)}$  and  $\mathbf{g}_r^{(t)}$ . Overall, as these angles widen beyond  $90^\circ$ , the magnitudes of the negative component  $\mathbf{g}_\parallel$  increases. It indicates that a greater portion of this components should be removed to fulfill the constraint specified in Eq. (7). In an extreme case where the angles approach  $180^\circ$ , nearly the entire  $\mathbf{g}_u^{(t)}$  is inverted relative to  $\mathbf{g}_r^{(t)}$ . It implies a substantial reduction in magnitudes of  $\mathbf{g}_u^{(t)}$  to approach 0 after adjustment.

## A.2 Proof of Theorem 3.1

*Proof.* To simply our symbology, we use  $\mathcal{L}(\boldsymbol{\theta})$  and  $\mathcal{R}(\boldsymbol{\theta})$  to replace  $\mathcal{L}(\mathcal{D}_u; \boldsymbol{\theta})$  and  $\mathcal{R}(\mathcal{D}_r; \boldsymbol{\theta})$  if raising no confusion. By the  $L$ -smoothness of  $\mathcal{L}$ , we have

$$\mathcal{L}(\boldsymbol{\theta}^{(t)} - \text{lr} \tilde{\mathbf{g}}_u^{(t)}) \leq \mathcal{L}(\boldsymbol{\theta}^{(t)}) - \text{lr} \mathbf{g}_u^{(t)\top} \tilde{\mathbf{g}}_u^{(t)} + \frac{L \text{lr}^2}{2} \|\tilde{\mathbf{g}}_u^{(t)}\|^2.$$

If we further define

$$\Delta^{(t)} := -\text{lr} \mathbf{g}_u^{(t)\top} \tilde{\mathbf{g}}_u^{(t)} + \frac{L \text{lr}^2}{2} \|\tilde{\mathbf{g}}_u^{(t)}\|^2.$$

Then, if  $\Delta^{(t)} < 0$ , we have a strict decrease, i.e.,  $\mathcal{L}(\boldsymbol{\theta}^{(t+1)}) < \mathcal{L}(\boldsymbol{\theta}^{(t)})$ , and thus we can complete our proof. As observed,  $\Delta^{(t)}$  consists of two terms:

- **Linear term:** Since  $\tilde{\mathbf{g}}_u^{(t)}$  is a projection of  $\mathbf{g}_u^{(t)}$  that does not invert the direction, we have  $\mathbf{g}_u^{(t)\top} \tilde{\mathbf{g}}_u^{(t)} \geq 0$ .
- **Quadratic term:** Since the norm of  $\tilde{\mathbf{g}}_u^{(t)}$  is bounded by  $\|\mathbf{g}_u^{(t)}\|$ , we have  $\frac{L \text{lr}^2}{2} \|\tilde{\mathbf{g}}_u^{(t)}\|^2 \leq \frac{L \text{lr}^2}{2} \|\mathbf{g}_u^{(t)}\|^2$ .

Hence the sign of  $\Delta^{(t)}$  depends on the term of  $-\text{lr} + \frac{L \text{lr}^2}{2}$ , where we need to ensure

$$-\text{lr} + L \text{lr}^2 / 2 < 0 \implies \text{lr} < 2/L.$$

Under the above condition, the negative linear term dominates the quadratic penalty term, so we have  $\Delta^{(t)} < 0$  and

$$\mathcal{L}(\boldsymbol{\theta}^{(t+1)}) < \mathcal{L}(\boldsymbol{\theta}^{(t)}).$$

Thus, we obtain a strict descent unless we encounter a degenerate scenario. Specifically, if  $\mathbf{g}_u^{(t)}$  happens to be exactly reversed with respect to the retain gradients  $\mathbf{g}_r^{(t)}$ , i.e. their angle is  $180^\circ$  and  $\cos(\mathbf{g}_u^{(t)}, \mathbf{g}_r^{(t)}) = -1$ , then, after rectification, one obtains  $\tilde{\mathbf{g}}_u^{(t)} = 0$ . In this case, we have  $\boldsymbol{\theta}^{(t+1)} = \boldsymbol{\theta}^{(t)}$ , which makes no further decrease. Thus, we complete the proof.  $\square$

## A.3 Proof of Theorem 3.3

*Proof.* Before giving the detailed proof, we first provide the following definition of the  $q$ -curvature.

**Definition A.1** ( $q$ -Curvature). For any smooth and differentiable loss  $\mathcal{R}$ , its  $q$ -Curvature with respect to some gradients  $\mathbf{g}$  is defined as

$$\mathfrak{H}_q(\mathcal{R}; \mathbf{g}) = \int_0^1 (1-a) [\mathbf{g}^\top \nabla^2 \mathcal{R}(\boldsymbol{\theta}^{(t)} - a \mathbf{g}) \mathbf{g}] da. \quad (16)$$

which quantifies the curvature of the local optimization landscape, with larger values indicating a sharper loss landscape.

Recall that at the  $t$ -th iteration, the original updating rule without GRU is  $\boldsymbol{\theta}_u^{(t+1)} = \boldsymbol{\theta}_u^{(t)} - \text{lr} \mathbf{g}_u^{(t)}$ . Additionally, according to the integral form of Taylor theorem, for any  $\alpha \in [0, 1]$ , we have

$$\mathcal{R}(\boldsymbol{\theta}^{(t)} - \text{lr} \mathbf{g}_u^{(t)}) = \mathcal{R}(\boldsymbol{\theta}^{(t)}) + \int_0^1 \nabla \mathcal{R}(\boldsymbol{\theta}^{(t)} - a \text{lr} \mathbf{g}_u^{(t)})^\top [-\text{lr} \mathbf{g}_u^{(t)}] da.$$

Separating the first-order (linear) portion and the second-order (Hessian) portion, one can write:

$$\mathcal{R}(\boldsymbol{\theta}_u^{(t+1)}) = \mathcal{R}(\boldsymbol{\theta}^{(t)}) - \text{lr} \langle \mathbf{g}_r^{(t)}, \mathbf{g}_u^{(t)} \rangle + \frac{1}{2} \int_0^1 [-\text{lr} \mathbf{g}_u^{(t)}]^\top \nabla^2 \mathcal{R}(\boldsymbol{\theta}^{(t)} - a \text{lr} \mathbf{g}_u^{(t)}) [-\text{lr} \mathbf{g}_u^{(t)}] da.$$

Since we assume  $\mathfrak{H}_{\text{lr}}(\mathcal{R}; \mathbf{g}_u^{(t)}) \geq \ell \|\mathbf{g}_u^{(t)}\|^2$ , we have

$$\int_0^1 [-\text{lr} \mathbf{g}_u^{(t)}]^\top \nabla^2 \mathcal{R}(\boldsymbol{\theta}^{(t)} - a \text{lr} \mathbf{g}_u^{(t)}) [-\text{lr} \mathbf{g}_u^{(t)}] da \geq \ell \text{lr}^2 \|\mathbf{g}_u^{(t)}\|^2,$$

and thus

$$\mathcal{R}(\boldsymbol{\theta}^{(t)} - \text{lr} \mathbf{g}_u^{(t)}) \geq \mathcal{R}(\boldsymbol{\theta}^{(t)}) - \text{lr} \langle \mathbf{g}_r^{(t)}, \mathbf{g}_u^{(t)} \rangle + \frac{\ell \text{lr}^2}{2} \|\mathbf{g}_u^{(t)}\|^2, \quad (17)$$

which establishes the lower bound for  $\mathcal{R}(\boldsymbol{\theta}_u^{(t+1)}) = \mathcal{R}(\boldsymbol{\theta}^{(t)} - \text{lr} \mathbf{g}_u^{(t)})$ . For the rectified updating rule with GRU, due to the  $L$ -smoothness, we have

$$\mathcal{R}(\boldsymbol{\theta}_{\text{gru}}^{(t+1)}) \leq \mathcal{R}(\boldsymbol{\theta}^{(t)}) - \text{lr} \langle \mathbf{g}_r^{(t)}, \tilde{\mathbf{g}}_u^{(t)} \rangle + \frac{L \text{lr}^2}{2} \|\tilde{\mathbf{g}}_u^{(t)}\|^2. \quad (18)$$

Combining Eq. (17) and Eq. (18), we have

$$\begin{aligned} \Delta &= \mathcal{R}(\boldsymbol{\theta}_u^{(t+1)}) - \mathcal{R}(\boldsymbol{\theta}_{\text{gru}}^{(t+1)}) \\ &\geq \underbrace{\left[ \mathcal{R}(\boldsymbol{\theta}^{(t)}) - \text{lr} \langle \mathbf{g}_r^{(t)}, \mathbf{g}_u^{(t)} \rangle + \frac{\ell \text{lr}^2}{2} \|\mathbf{g}_u^{(t)}\|^2 \right]}_{\text{Lower bound for } \mathcal{R}(\boldsymbol{\theta}_u^{(t+1)})} - \underbrace{\left[ \mathcal{R}(\boldsymbol{\theta}^{(t)}) - \text{lr} \langle \mathbf{g}_r^{(t)}, \tilde{\mathbf{g}}_u^{(t)} \rangle + \frac{L \text{lr}^2}{2} \|\tilde{\mathbf{g}}_u^{(t)}\|^2 \right]}_{\text{Upper bound for } \mathcal{R}(\boldsymbol{\theta}_{\text{gru}}^{(t+1)})}. \end{aligned}$$

After organizing, we have

$$\begin{aligned} \Delta &\geq \left[ -\text{lr} \langle \mathbf{g}_r^{(t)}, \mathbf{g}_u^{(t)} \rangle + \frac{\ell \text{lr}^2}{2} \|\mathbf{g}_u^{(t)}\|^2 \right] - \left[ -\text{lr} \langle \mathbf{g}_r^{(t)}, \tilde{\mathbf{g}}_u^{(t)} \rangle + \frac{L \text{lr}^2}{2} \|\tilde{\mathbf{g}}_u^{(t)}\|^2 \right] \\ &= \underbrace{-\text{lr} \langle \mathbf{g}_r^{(t)}, \mathbf{g}_u^{(t)} \rangle + \text{lr} \langle \mathbf{g}_r^{(t)}, \tilde{\mathbf{g}}_u^{(t)} \rangle}_{\text{(linear-difference term)}} + \underbrace{\frac{\ell \text{lr}^2}{2} \|\mathbf{g}_u^{(t)}\|^2 - \frac{L \text{lr}^2}{2} \|\tilde{\mathbf{g}}_u^{(t)}\|^2}_{\text{(quadratic-difference term)}}. \end{aligned}$$

Now, we show that the formulations inside each bracket is non-negative:

1. **Rectification Nonnegativity.** Since  $\tilde{\mathbf{g}}_u^{(t)}$  is formed from  $\mathbf{g}_u^{(t)}$  by removing negatively aligned components with respect to  $\mathbf{g}_r^{(t)}$ , we have  $\langle \mathbf{g}_r^{(t)}, \tilde{\mathbf{g}}_u^{(t)} \rangle \geq \langle \mathbf{g}_r^{(t)}, \mathbf{g}_u^{(t)} \rangle$ , and thus  $-\langle \mathbf{g}_r^{(t)}, \mathbf{g}_u^{(t)} \rangle + \langle \mathbf{g}_r^{(t)}, \tilde{\mathbf{g}}_u^{(t)} \rangle \geq 0$ . Multiplication by  $\text{lr}$  preserves non-negativity, ensuring that the expression inside the first bracket remains non-negative.
2. **Curvature Conditions.** Due to conditions **a)**-**b)**, we have  $\ell \geq \frac{\|\mathbf{g}_u^{(t)} - \mathbf{g}_r^{(t)}\|^2}{\|\mathbf{g}_u^{(t)} + \mathbf{g}_r^{(t)}\|^2} L$  and  $\ell \geq \frac{\|\mathbf{g}_u^{(t)} - \mathbf{g}_r^{(t)}\|^2}{\|\mathbf{g}_u^{(t)} + \mathbf{g}_r^{(t)}\|^2} L + \frac{2}{\text{lr}}$ , which further indicate that  $\frac{\ell \text{lr}^2}{2} \|\mathbf{g}_u^{(t)}\|^2 - \frac{L \text{lr}^2}{2} \|\tilde{\mathbf{g}}_u^{(t)}\|^2 \geq 0$ , so the second bracket is also non-negative.

Thus we complete the proof.  $\square$

Table 6: Full experimental results on the TOFU benchmarks: Evaluating 5% and 10% unlearning setups across different backbones and baseline methods. The results are presented in two adjacent rows for each method, one row (original baseline method name) showing the original results and the other (w/ GRU) displaying the results combined with GRU. The superior results between configurations with and without GRU for each baseline method are highlighted in **bold**.

Method	Phi-1.5				LLaMA2-7B			
	5%		10%		5%		10%	
	FQ↑	MU↑	FQ↑	MU↑	FQ↑	MU↑	FQ↑	MU↑
Original	-28.8476	0.5200	-40.5243	0.5200	-32.1330	0.6332	-48.5895	0.6332
Retrain	0.0000	0.5250	0.0000	0.5320	0.0000	0.6006	0.0000	0.6137
GA	-28.0555	0.0000	-28.5669	0.0000	-16.9281	0.0000	-14.3716	0.0000
w/ GRU	<b>-5.1004</b>	<b>0.3587</b>	<b>-11.3678</b>	<b>0.2482</b>	<b>-3.5161</b>	<b>0.5190</b>	<b>-12.1912</b>	<b>0.3108</b>
WGA	-12.4230	0.0284	-29.8615	0.0063	-7.7503	0.4447	-28.5669	0.1154
w/ GRU	<b>-1.9514</b>	<b>0.4431</b>	<b>-6.6882</b>	<b>0.4184</b>	<b>-5.1004</b>	<b>0.5698</b>	<b>-19.7868</b>	<b>0.5107</b>
NPO	-11.9082	0.3565	-15.7638	0.3267	-10.9105	0.4919	-8.7037	0.2876
w/ GRU	<b>-0.9326</b>	<b>0.3935</b>	<b>-3.1620</b>	<b>0.3714</b>	<b>-9.9550</b>	<b>0.5408</b>	<b>-2.5106</b>	<b>0.4570</b>
GD	-6.5526	0.4061	-50.2968	0.2999	-13.4847	0.5549	-13.9215	0.3930
w/ GRU	<b>-5.8059</b>	<b>0.4138</b>	<b>-13.4785</b>	<b>0.4096</b>	<b>-12.4230</b>	<b>0.5637</b>	<b>-11.7760</b>	<b>0.5407</b>
NPO+KL	-11.9082	0.3634	-17.2193	0.3444	-10.4275	0.5094	-9.4304	0.3109
w/ GRU	<b>-0.0360</b>	<b>0.3833</b>	<b>-3.1620</b>	<b>0.3654</b>	<b>-10.4275</b>	<b>0.5585</b>	<b>-2.1101</b>	<b>0.4480</b>
NPO+GD	-12.4230	0.4002	-19.7868	0.4026	-11.9082	0.5256	-12.6133	0.4750
w/ GRU	<b>-9.4931</b>	<b>0.4514</b>	<b>-7.6651</b>	<b>0.4122</b>	<b>-8.1703</b>	<b>0.5673</b>	<b>-2.9381</b>	<b>0.5000</b>
SimNPO+GD	-12.9485	0.4428	-26.6801	0.4523	-9.0417	0.5073	-9.8040	0.5527
w/ GRU	<b>-12.9485</b>	<b>0.4862</b>	<b>-25.4588</b>	<b>0.4934</b>	<b>-9.0417</b>	<b>0.5516</b>	<b>-9.4304</b>	<b>0.6168</b>

## B Detailed Results

This section provides comprehensive results that echo our main experiments discussed in Section 5.1. It encompasses TOFU, WMDP, and MUSE benchmarks, further incorporating additional baseline methods like SimNPO, and other metrics, such as VerbMem for MUSE. These results are summarized in Tables 6-8.

Overall, we still conclude that GRU is capable to reliably mitigate the trade-off between removal and retention, typically showing improvements for all the metrics that align with each goal. Note that, we also observe that in some situations, the enhancements in preserving overall model performance occur at the expense of decreased strength of removal, particularly for those results on WMDP and MUSE. Fortunately, this scenario occurs only for certain specific metrics, and the decrease in the efficacy of removal appears to be negligible when compared to the substantial improvements in retention. Therefore, we still consider our GRU as an effective solution to mitigate the trade-off and enhance the overall unlearning efficacy.

Table 7: Detailed experimental results on the WMDP benchmarks with QA accuracies evaluated on Bio unlearning and MMLU using the ZEPHYR-7B-BETA backbone. The results are presented in two adjacent rows for each method, one row (original baseline method name) showing the original results and the other (w/ GRU) displaying the results combined with GRU. The superior results between configurations with and without GRU for each baseline method are highlighted in **bold**.

Method	Unlearning		Retention
	Bio ↓	Cyber ↓	MMLU ↑
Original	0.6371	0.4383	0.5814
GA	<b>0.2474</b>	<b>0.2431</b>	0.2465
w/ GRU	<b>0.2474</b>	0.2446	<b>0.2852</b>
WGA	0.2476	0.2647	0.2454
w/ GRU	<b>0.2474</b>	<b>0.2587</b>	<b>0.2604</b>
GD	<b>0.2474</b>	<b>0.2441</b>	0.2589
w/ GRU	<b>0.2474</b>	0.2511	<b>0.2995</b>
NPO	0.2655	<b>0.2793</b>	0.3033
w/ GRU	<b>0.2561</b>	<b>0.2793</b>	<b>0.3704</b>
NPO+GD	0.2710	<b>0.3493</b>	0.4724
w/ GRU	<b>0.2639</b>	0.3524	<b>0.5033</b>

Table 8: Detailed experimental results on the MUSE benchmarks with KnowMem, assessing the efficacy of removal and retention on targeted and non-targeted data, respectively. The results are presented in two adjacent rows for each method, one row (original baseline method name) showing the original results and the other (w/ GRU) displaying the results combined with GRU. The superior results between configurations with and without GRU for each baseline method are highlighted in **bold**.

Method	VerbMem ↓	KnowMem-U ↓	KnowMem-R ↑
Original	99.7016	45.8791	69.4009
Retrain	13.8896	30.1380	69.0496
GA	<b>0.0000</b>	<b>0.0000</b>	0.0000
w/ GRU	<b>0.0000</b>	<b>0.0000</b>	<b>6.7006</b>
WGA	0.2284	<b>0.0000</b>	0.0000
w/ GRU	<b>0.0198</b>	<b>0.0000</b>	<b>18.4555</b>
GD	<b>0.0000</b>	<b>0.0000</b>	8.6971
w/ GRU	<b>0.0000</b>	<b>0.0000</b>	<b>9.8586</b>
NPO	<b>0.0000</b>	<b>0.0000</b>	0.0000
w/ GRU	<b>0.0000</b>	<b>0.0000</b>	<b>9.5913</b>
NPO+GD	<b>0.0000</b>	<b>0.0000</b>	23.5565
w/ GRU	<b>0.0000</b>	<b>0.0000</b>	<b>30.7492</b>

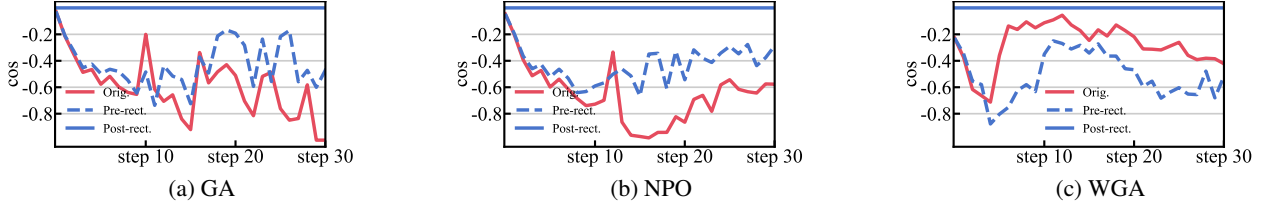


Figure 7: Angles between  $\mathbf{g}_u^{(t)}$  and  $\mathbf{g}_r^{(t)}$  (labeled ‘Orig.’ for the original baseline and ‘Pre-rect.’ for the GRU-enhanced baseline) and between  $\tilde{\mathbf{g}}_u^{(t)}$  and  $\mathbf{g}_r^{(t)}$  (labeled ‘Post-rect.’ for the GRU-enhanced baseline) across various unlearning steps. We evaluate the baseline methods NPO, GA, and WGA in a 5% TOFU setup using the Llama-2-7B model.

### C Hyper-parameter Configurations

In addition to our main results, we further discuss about our hyper-parameter configurations. We employ grid search on validation data to select proper hyper-parameters for GRU and TRU. For GRU, the candidate values for  $\gamma$  include  $\{0.01, 0.05, 0.1, 0.2, 0.3, 0.4, 0.5, 0.6, 0.7, 0.8, 0.9, 0.99\}$ , and that for  $\tau$  are  $\{0.001, 0.005, 0.01, 0.1, 1.0, 10, 100\}$ . For TRU, we select  $\text{stg}$  from the space  $\{0.50, 0.60, 0.65, 0.70, 0.75, 0.80, 0.85\}$  while fix  $\text{lr} = 1e^{-4}$ . We further summarize their detailed configurations across different setups as follows.

**GRU.** For TOFU with Phi-1.5, we default to set  $\tau = 0.001$ , while adjusting  $\tau = 0.01$  for the 5% setup and without using gradient clipping for GD. For TOFU with Llama-2-7B, we do not use gradient clipping for GA, GD, NPO, and SimNPO under the 5% setup, while setting  $\tau = 1.0$  for all other methods. In the 10% setup,  $\tau = 1.0$  for GA, WGA, GD, SimNPO, and NPO+GD;  $\tau = 0.5$  for NPO;  $\tau = 0.1$  for NPO+KL. For WMDP,  $\tau = 1.0$  for GA;  $\tau = 0.01$  for NPO and NPO+GD;  $\tau = 0.001$  for GD and WGA. For MUSE,  $\tau = 1.0$  for GA, GD and WGA;  $\tau = 100$  for NPO and NPO+GD.

For TOFU, we by default set  $\gamma = 0.8$ , while setting  $\gamma = 0.05$  with Llama-2-7B and  $\gamma = 0.1$  with Phi. Also, we set  $\gamma = 0.5$  for SimNPO. Moreover, we set  $\gamma = 0.8$  for MUSE and  $\gamma = 0.99$  for WMDP.

**TRU.** With the backbone of Phi-1.5, we set  $\text{stg} = 0.7$  under the 5% setup and  $\text{stg} = 0.75$  under the 10% setup. Also, with the backbone of Llama-2-7B, we set  $\text{stg} = 0.65$  under the 5% setup and  $\text{stg} = 0.85$  under the 10% setup.

### D Other Analyses

We provide more analyses to further show the respective effects of different components involved in our algorithm design.

#### D.1 Visualization of Rectification.

We further examine the angles between  $\mathbf{g}_u^{(t)}$  and  $\mathbf{g}_r^{(t)}$ , along with those results after being rectified via GRU. We monitor the dynamics of these angles throughout the unlearning processes for various baseline methods, as well as the changes after applying GRU for rectification. As a case study, Figure 7 shows these results on TOFU 5% unlearning with Llama-2-7B as the backbone. Without the use of GRU, the cosine similarity between  $\mathbf{g}_u^{(t)}$  and  $\mathbf{g}_r^{(t)}$  keeps negative throughout unlearning, suggesting potential adverse effects on the overall performance of the model. In comparison, within the unlearning dynamics facilitated by GRU, it is observed that although the angles initially continue to be negative (dotted lines), our rigorous method of gradient rectification will adjust the resulting cosine similarity to exactly 0. This adjustment ensures that the gradient direction associated with unlearning is completely orthogonal to that of retention, thereby effectively maintaining the overall model performance.

#### D.2 Further Strategy

We further introduce a strategy to mitigate potential side effects when the unlearning and retention gradients become nearly antiparallel. We first describe the method in detail and then present its tuning results, demonstrating its impact on unlearning stability and overall model performance.

**Angle Clipping for Gradient Updates.** In cases where the unlearning gradient  $\mathbf{g}_u^{(t)}$  and the retention gradient  $\mathbf{g}_r^{(t)}$  are nearly antiparallel (i.e.,  $\cos(\mathbf{g}_u^{(t)}, \mathbf{g}_r^{(t)}) \approx -1$ ), directly applying our gradient adjustment from Eq. (8) can result in an

Table 9: Hyper-parameter turning of  $c$  on TOFU with Llama-2-7B, under the 5% unlearning setup. The notation “-” indicates that the associated result is same to those without GRU.

Method	Metric	$c$						
		-0.08	-0.1	-0.4	-0.5	-0.6	-0.8	N/A
GA w/ GRU	FQ $\uparrow$	-4.7631	-5.4480	-6.9414	-8.1703	-7.7503	-7.3407	-8.6008
	MU $\uparrow$	0.4300	0.4362	0.5194	0.5420	0.5667	0.5725	0.5810
NPO w/ GRU	FQ $\uparrow$	-8.1703	-6.1741	-12.4230	-8.6008	-9.0417	-	-9.0417
	MU $\uparrow$	0.4307	0.3621	0.5396	0.5207	0.5284	-	0.5220
GD w/ GRU	FQ $\uparrow$	-13.4850	-12.9485	-	-	-	-	-12.4230
	MU $\uparrow$	0.5624	0.5637	-	-	-	-	0.5637

extreme directional shift. Consequently, the magnitude of the updated gradient  $\tilde{\mathbf{g}}_u^{(t)}$  may shrink excessively, halting meaningful progress on unlearning objectives. This issue effectively stalls model updates and compromises the desired unlearning trajectory. To address the aforementioned risk of vanishing updates, we impose a constraint by setting a minimal-allowed value  $c$  on  $\cos(\mathbf{g}_u^{(t)}, \mathbf{g}_r^{(t)})$ . Specifically, when  $\cos(\mathbf{g}_u^{(t)}, \mathbf{g}_r^{(t)}) < c$ , we clip the cosine term such that:

$$\cos(\mathbf{g}_u^{(t)}, \mathbf{g}_r^{(t)}) \leftarrow \max(\cos(\mathbf{g}_u^{(t)}, \mathbf{g}_r^{(t)}), c).$$

By preventing  $\cos(\mathbf{g}_u^{(t)}, \mathbf{g}_r^{(t)})$  from dropping below  $c$ , the updated gradient avoids undesirably large rotations. This ensures more stable and controlled progress for GRU-based methods in an unlearning setup.

**Tuning Results.** To investigate how angle clipping affects both unlearning and retention, we performed a series of experiments on the TOFU dataset under a 5% unlearning setup (Table 9). We varied  $c$  across several negative thresholds— $-0.08$ ,  $-0.1$ ,  $-0.4$ ,  $-0.5$ ,  $-0.6$ ,  $-0.8$ —and compared these against a baseline with no clipping (N/A). We evaluated performance based on two metrics: FQ and MU. Our observations suggest that moderately negative thresholds (e.g.,  $-0.4$  to  $-0.5$ ) tend to strike a better balance, offering stable unlearning progress without overly compromising retention. When  $c$  is set to a small negative value (e.g.,  $-0.08$ ), the resulting gradients can become too constrained, limiting the model’s ability to forget. By contrast, highly negative  $c$  (e.g.,  $-0.8$ ) may trigger abrupt directional changes, potentially eroding retention. In practice, when stronger unlearning is prioritized, one may opt for a more negative threshold, whereas settings closer to 0 can help preserve model utility. Users are encouraged to tune  $c$  on a validation set, selecting the threshold that appropriately balances unlearning effectiveness with overall model performance.

**Algorithm 2** TRU Framework

---

```

1: Input: Initial parameters  $\theta_{\text{org}}$ , learning rate  $\text{lr}$ , number of iterations  $T$ , hyperparameter  $\text{stg}$ , and unlearning
   dataset  $\mathcal{D}_u$ .
2: // Initialize the aggregated (rectified) task vector.
3:  $\tilde{\mathbf{T}}_{\mathcal{D}_u} \leftarrow \mathbf{0}$ .
4: for each data point  $s_u \in \mathcal{D}_u$  do
5:   // 1) Compute the “targeted” task vector for  $s_u$ .
6:    $\mathbf{T}_{s_u} \leftarrow \text{COMPUTETARGETEDTASKVECTOR}(s_u; \theta_{\text{org}})$ ;
7:   // 2) Compute the “retain” task vector by finetuning on  $\mathcal{D}_u \setminus \{s_u\}$ .
8:    $\mathbf{T}_{\text{ret}} \leftarrow \text{COMPUTERETAINTASKVECTOR}(\mathcal{D}_u \setminus \{s_u\}; \theta_{\text{org}})$ ;
9:   // 3) Check for conflict: if  $-\mathbf{T}_{s_u}$  negatively impacts  $\mathbf{T}_{\text{ret}}$ , perform rectification.
10:  if  $\langle -\mathbf{T}_{s_u}, \mathbf{T}_{\text{ret}} \rangle < 0$  then
11:     $\tilde{\mathbf{T}}_{s_u} \leftarrow \mathbf{T}_{s_u} + \frac{[\langle \mathbf{T}_{s_u}, \mathbf{T}_{\text{ret}} \rangle]_-}{\|\mathbf{T}_{\text{ret}}\|^2} \mathbf{T}_{s_u}$ .
12:  else
13:     $\tilde{\mathbf{T}}_{s_u} \leftarrow \mathbf{T}_{s_u}$ .
14:  end if
15:  // 4) Accumulate rectified task vectors for all points in  $\mathcal{D}_u$ .
16:   $\tilde{\mathbf{T}}_{\mathcal{D}_u} \leftarrow \tilde{\mathbf{T}}_{\mathcal{D}_u} + \tilde{\mathbf{T}}_{s_u}$ .
17: end for
18: // 5) Apply the aggregated (rectified) vector once, scaled by  $\text{stg}/n$ .
19:  $\theta_{\text{TRU}} \leftarrow \theta_{\text{org}} - \frac{\text{stg}}{n} \tilde{\mathbf{T}}_{\mathcal{D}_u}$ .
20: Return  $\theta_{\text{TRU}}$ .

```

---

**E TRU Algorithm Implementation**

We present the implementation details of our TRU algorithm in Algorithm 2. TRU removes knowledge from a targeted dataset without mini-batches or iterative accumulations. Specifically, it processes each data point  $s_u$  in the unlearning set  $\mathcal{D}_u$  just once. For each data point, TRU computes a *task vector*  $\mathbf{T}_{s_u}$  to capture the shift in parameters needed to learn  $s_u$  from the original model  $\theta_{\text{org}}$ . Then, rather than relying on a gradient over  $\mathcal{D}_u \setminus \{s_u\}$ , the *retain* step refines the model by computing a separate *retain task vector*  $\mathbf{T}_{\text{ret}}$  through finetuning on the remaining unlearning samples, indicating how to preserve overall performance. If negating  $\mathbf{T}_{s_u}$  conflicts with  $\mathbf{T}_{\text{ret}}$ , we remove the problematic directional component via rectification, yielding a rectified vector  $\tilde{\mathbf{T}}_{s_u}$ . We accumulate these rectified vectors over all points in  $\mathcal{D}_u$ , and finally apply a *single* large-scale update to subtract the aggregate unlearning direction from the original parameters, scaled by a hyperparameter  $\text{stg}$ . In practical scenarios, to reduce computational overhead, we partition  $\mathcal{D}_u$  into multiple subsets rather than iterating over each individual data point  $s_u$ .